

Light control with Weyl semimetals

Cheng Guo^{1*†}, Viktor S. Asadchy^{2,3*}, Bo Zhao^{4*} and Shanhui Fan^{2^}

Full list of author information is available at the end of the article

*Equal contributor

†Correspondence:

guocheng@stanford.edu

^Correspondence:

shanhui@stanford.edu

Abstract

Weyl semimetals are topological materials whose electron quasiparticles obey the Weyl equation. They possess many unusual properties that may lead to new applications. This is a tutorial review of the optical properties and applications of Weyl semimetals. We review the basic concepts and optical responses of Weyl semimetals, and survey their applications in optics and thermal photonics. We hope this pedagogical text will motivate further research on this emerging topic.

Keywords: Weyl semimetal; topological materials; axion electrodynamics; nanophotonics; thermal photonics; optical nonreciprocity

Introduction

Weyl semimetals are topological materials whose low-energy excitations obey the Weyl equation [1, 2]. In a Weyl semimetal, the conduction and valence bands touch at discrete points in momentum space, called Weyl nodes. Weyl nodes are monopoles of the Berry curvature and are robust under generic perturbations. The quasiparticles near the Weyl nodes are analogous to Weyl fermions in high-energy physics [3]; they exhibit linear dispersion and well-defined chirality.

The nontrivial topology of Weyl semimetals leads to many unusual electronic, magnetic, thermal, and optical properties [2, 4, 5]. These intriguing features have been extensively studied in the literature. Besides these fundamental interests, Weyl semimetals may also enable new opportunities in practical applications. For example, photonic applications include compact optical isolators and circulators [6, 7, 8], orbital angular momentum detectors [9, 10], higher-order harmonic generation [11, 12, 13], and nonreciprocal thermal emitters [14, 15, 16] among many others. However, such an application-oriented exploration is still at an early stage, which requires more joint efforts from scientists and engineers.

This text is a tutorial review of Weyl semimetals that should be of interest to researchers working in photonics, applied physics, and optical engineering. We start with the basic concepts of semimetals and Weyl semimetals (Sec. 1). Then, we review the formalism of axion electrodynamics and derive the optical responses of Weyl semimetals (Sec. 2). Next, we survey the broad potential applications of Weyl semimetals in optics (Sec. 3). Finally, we discuss the applications of Weyl semimetals in thermal photonics (Sec. 4). We hope that our survey will motivate further exploration of photonic applications with Weyl semimetals.

1 Semimetals and Weyl semimetals

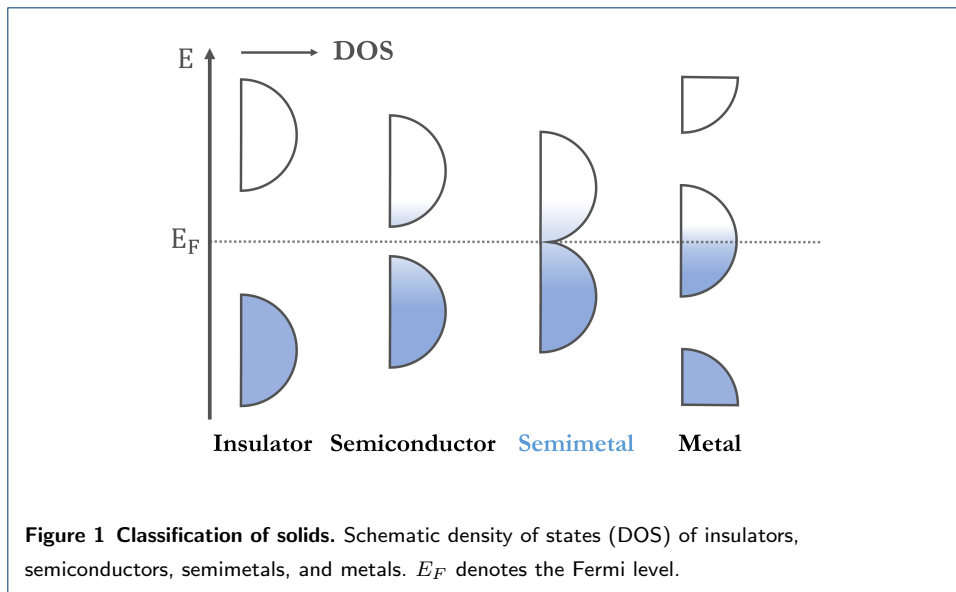
Weyl semimetals are a special class of semimetals. They exhibit common properties of semimetals as well as some unique characteristics. This section provides a brief introduction to semimetals and Weyl semimetals. In Sec. 1.1, we review the basic concept and common properties of semimetals. We also discuss typical behaviors and material examples of conventional semimetals. In Sec. 1.2, we review the basic concept and physical properties of Weyl semimetals.

1.1 Semimetals

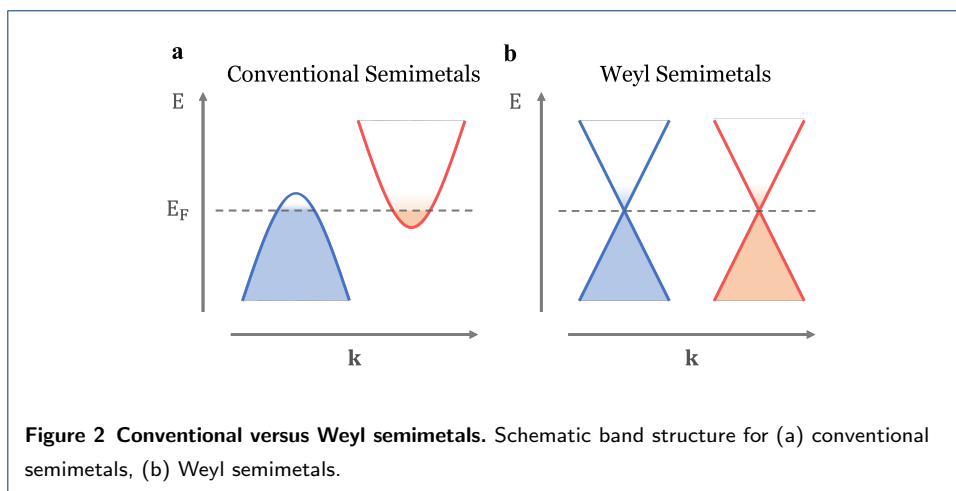
According to the band theory [17, 18], solids can be classified as insulators, semiconductors, semimetals, and metals (Fig. 1). An insulator or a semiconductor has a band gap between the valence and conduction bands; the band gap is larger for an insulator ($>4\text{eV}$) than for a semiconductor ($<4\text{eV}$). A *semimetal* has a very small overlap between the conduction and valence bands and a negligible density of states at the Fermi level. A metal has a partially filled conduction band and an appreciable density of states at the Fermi level.

Different band structures lead to different physical properties. For example, the carrier concentration is $>10^{22}\text{cm}^{-3}$ for normal metals, $\sim 10^{17}\text{--}10^{20}\text{cm}^{-3}$ for semimetals, and $\sim 10^6\text{--}10^{13}\text{cm}^{-3}$ for intrinsic semiconductors such as GaAs, Si, and Ge. Consequently, the electrical conductivities are $\sim 10^5\text{--}10^6\ \Omega^{-1}\text{cm}^{-1}$ for normal metals, $\sim 10^4\ \Omega^{-1}\text{cm}^{-1}$ for semimetals, and $\sim 10^{-8}\text{--}10^{-1}\ \Omega^{-1}\text{cm}^{-1}$ for intrinsic semiconductors [18].

Semimetals, the focus of our study, are probably the least known among the four types. An intrinsic semimetal has an equal number of electrons and holes. Like a normal metal, its conductivity increases as the temperature is lowered. Like



a semiconductor, it can be doped with proper impurities to vary the number of electrons and holes. Its electronic properties are also sensitive to pressure since pressure changes the internuclear distances, which sensitively changes the amount of band overlap and causes large changes in the carrier concentrations. Besides low carrier concentrations, semimetals typically have small effective masses and high dielectric constants. Nonmagnetic semimetals typically exhibit high diamagnetic susceptibilities and huge electron g -values [18].



A conventional semimetal is a “semiconductor” with a negative indirect bandgap (Fig. 2a). In an intrinsic semimetal, the bottom of the conduction band is slightly lower than the top of the valence band, and the Fermi level sits in between. Hence,

the semimetal has charge carries of both types (holes and electrons). Typically, the pockets of electrons and holes are located at different positions in the wavevector space [18].

Classic examples of semimetals include the group 5A elements: arsenic, antimony, and bismuth [18]. They have five valence electrons per atom, so if there were one atom per primitive cell the material would be a metal. However, there are two atoms per primitive cell. With the ten valence electrons, the crystal could be an insulator but there is a small overlap in energy between the conduction and valence bands, resulting in semimetal behavior [19].

Another well-known semimetal is graphite. It consists of stacked layers of graphene. Since the interlayer bonding is very weak, the band overlap is tiny [20]. Hence, graphite is a semimetal, and the Fermi surface consists primarily of tiny pockets of electrons and holes at different wavevectors, with carrier densities of around $n_e = n_h = 3 \times 10^{18} \text{ cm}^{-3}$ [17].

1.2 Weyl semimetals

Weyl semimetals are a unique class of semimetals. Unlike conventional semimetals, in Weyl semimetals, the valence and conduction bands touch at discrete points in the wavevector space. Near the touching point, the band dispersion is linear (Fig. 2b).

Weyl semimetals are named after Hermann Weyl (1885-1955). In 1929, Weyl proposed the Weyl equation [21], which simplifies the Dirac equation for a *massless* relativistic spin $\frac{1}{2}$ particle:

$$i\hbar \frac{\partial \Psi}{\partial t} = \hat{H} \Psi = \pm c \mathbf{p} \cdot \boldsymbol{\sigma} \Psi. \quad (1)$$

Here \hbar is the reduced Planck constant, c is the speed of light, $\mathbf{p} = (p_x, p_y, p_z)$ is the momentum operator, $\boldsymbol{\sigma} = (\sigma_x, \sigma_y, \sigma_z)$ is a vector whose components are the Pauli matrices, and Ψ is a two-component field called a Weyl spinor [3]. The Weyl equation describes a massless particle with linear dispersion, called a Weyl fermion. The \pm sign reflects the existence of two types of Weyl fermions: right-handed (+) and left-handed (-). Hence, unlike the Dirac equation, the Weyl equation violates parity.

Physicists have been searching for Weyl fermions in nature. However, none of the observed elementary particles are Weyl fermions [2]. It was thought that neutrinos

could be Weyl fermions. However, the discovery of neutrino oscillation in 1998 [22] shows that neutrinos are massive and thus cannot be Weyl fermions.

Despite their absence in high-energy physics, Weyl fermions may be realized in condensed-matter systems. In 1937, Conyers Herring proposed the concept of Weyl semimetals [1]. He realized that when two electronic bands cross accidentally, the generic band dispersions near a touching point are linear in all directions. In the simplest scenario, the effective Hamiltonian reads [23]:

$$\hat{H} = \pm v_F \mathbf{p} \cdot \boldsymbol{\sigma} \quad (2)$$

where \mathbf{p} is the momentum deviation from the touching point, and v_F is the Fermi velocity. The resemblance between Eqs. (1) and (2) is evident. As a result, these touching points are called Weyl nodes, and the quasiparticles near them are reminiscent of Weyl fermions. Each Weyl point has a definite chirality, either right-handed (+) or left-handed (−). For crystals where the wavevector space is the Brillouin zone and hence is compact, the Nielsen-Ninomiya no-go theorem asserts that left- and right-handed Weyl points always appear in pairs [24, 25, 26, 27]. Hence, it is impossible that only a single Weyl point exists in the momentum space for solid state systems.

Weyl points are robust to generic perturbations: The Hamiltonian remains gapless while Weyl nodes move around. This is because for a Hermitian matrix, having a pair of coalescing eigenvalues is an effect with codimension three; generically, one needs to tune three real parameters to realize such an effect. This fact, known as the von Neumann-Wigner theorem [28], explains why generically the accidental degeneracies of two bands only occur at isolated points in the three-dimensional momentum space and why such degeneracies persist under perturbation. From a topological perspective, the robustness of Weyl points can be understood from Berry curvature [29]. Berry curvature arises from the variation of the periodic part of the Bloch wave function with respect to wavevectors, and is mathematically analogous to a magnetic field in momentum space. Weyl points are monopoles of Berry curvature with quantized charges, which are analogous to quantized magnetic monopoles for magnetic fields. Weyl points can only be destroyed when two Weyl nodes of opposite chiralities are moved together and annihilated with each other.

For a Weyl semimetal, the existence of Weyl nodes in the bulk band structure leads to the presence of Fermi arc surface states when the Weyl semimetal is truncated. Such surface states correspond to an open Fermi arc that connects the projection in the surface Brillouin zone of two Weyl nodes of opposite chiralities. The existence of such surface Fermi arcs is protected by the nontrivial chiral charge of the Weyl nodes [30, 31]. This is an example of the general principle of bulk-boundary correspondence in topological materials.

Although the Weyl semimetal was theoretically proposed many decades ago, its experimental demonstration was quite recent. A material must satisfy some necessary conditions to be a potential candidate for Weyl semimetals [32]. First, it must break either time-reversal or spatial inversion symmetry [2]. In a system that satisfies both time-reversal and spatial inversion symmetry, all the bands must be doubly degenerate in the whole wavevector space due to the Kramers' degeneracy theorem [33]; this excludes the existence of Weyl nodes, which only appear as the accidental degeneracy of two non-degenerate bands. The minimum numbers of Weyl nodes are 2 and 4 for Weyl semimetals that break time-reversal symmetry and inversion symmetry, respectively. Second, the Weyl nodes must be located near the Fermi level, so that Weyl fermions may emerge as low-energy excitations.

Weyl semimetals were first discovered in 2015 [34, 35] in non-centrosymmetric crystals, TaAs family (TaAs [34, 35], TaP [36, 37], NbAs [38], and NbP [39, 40, 41]). Later, magnetic Weyl semimetals that break time-reversal symmetry have also been discovered [42, 43, 44]. A number of other Weyl semimetals have since been discovered, as reviewed in Ref. [45].

Weyl semimetals exhibit a rich variety of novel phenomena. Besides surface Fermi arc states, they also exhibit chiral anomaly [46, 47, 48], unconventional charge and heat transport [49, 41], strain-induced axial gauge fields [50, 51, 52], novel collective modes [53], and so on. The properties of Weyl semimetals have been summarized in numerous reviews and monographs: For general overviews, see Refs. [54, 2, 55]; for electronic properties, see Ref. [4]; for magnetic properties, see Refs. [56, 57, 58]; for transport properties, see Refs. [59, 60, 61, 62, 63, 64]; for topological properties, see Refs. [65, 66]; for *ab initio* calculation, see Ref. [67]; for experimental studies, see Ref. [68, 69, 70, 71]; for material properties, see Ref. [45]. Complementary to

these works, the present tutorial review will focus on the optical properties of Weyl semimetals.

2 Optical properties of Weyl semimetals

In this section, we derive the linear optical properties of Weyl semimetals. We consider the simplest Weyl semimetal with two nodes separated by $2\mathbf{b}$ in their wavevectors and $2\hbar b_0$ in their energy (Fig. 3a). The constitutive relations for such an ideal Weyl semimetal are:

$$\mathbf{D} = \varepsilon_D(\omega)\mathbf{E} + \frac{i e^2}{2\pi^2 \hbar \omega} (-b_0 \mathbf{B} + \mathbf{b} \times \mathbf{E}), \quad \mathbf{H} = \frac{1}{\mu_0} \mathbf{B}. \quad (3)$$

The derivation of Eq. (3) is the main aim of this section. The expression of \mathbf{D} has two terms; the first term is referred to as the Dirac term and the second the axion term. The Dirac term describes the permittivity of a corresponding Dirac semimetal (Fig. 3b), i.e., a Weyl semimetal with two overlapping Weyl nodes ($\mathbf{b} = \mathbf{0}, b_0 = 0$). The axion term captures the effects of Weyl node separation. Its name is taken from axion electrodynamics. Its first term represents the chiral magnetic effect, while the second term represents the anomalous Hall effect [72, 2].

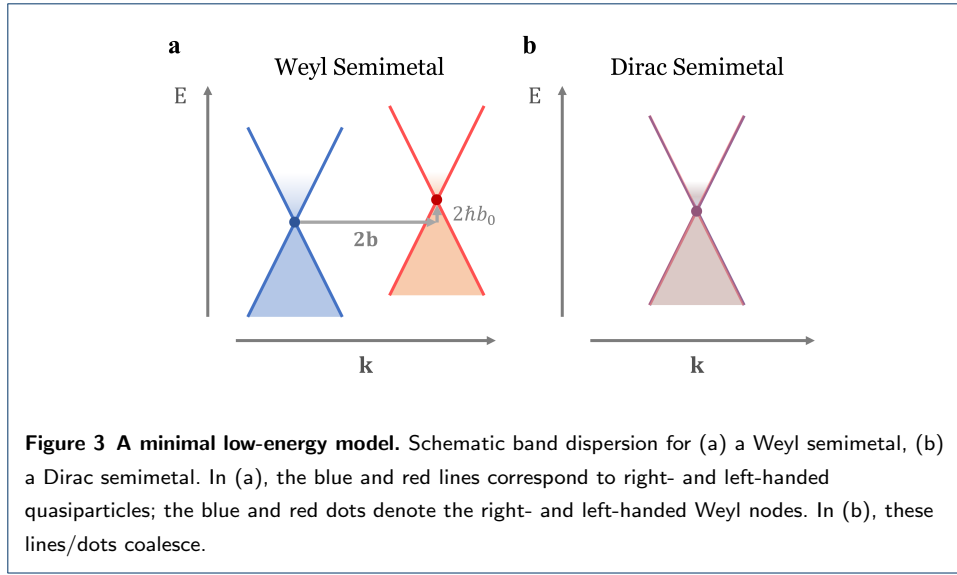
In the following subsections, we provide a step-by-step derivation of Eq. (3) and a closed-form expression of $\varepsilon_D(\omega)$. Then we discuss their physical consequences. We use SI units and $e^{-i\omega t}$ convention.

2.1 A minimal low-energy model of Weyl semimetals

According to the Nielsen-Ninomiya theorem [24, 25, 26], a Weyl semimetal always include an even number of Weyl nodes and the total chirality of all nodes must vanish. Hence, the simplest Weyl semimetal has a single pair of Weyl nodes. It can be described by the following minimal low-energy Hamiltonian:

$$H = \begin{pmatrix} \hbar v_F \boldsymbol{\sigma} \cdot (\mathbf{k} + \mathbf{b}) - \hbar b_0 I & 0 \\ 0 & -\hbar v_F \boldsymbol{\sigma} \cdot (\mathbf{k} - \mathbf{b}) + \hbar b_0 I \end{pmatrix}, \quad (4)$$

which characterizes two Weyl nodes of opposite chirality that are separated by $2\mathbf{b}$ in wavevector and $2\hbar b_0$ in energy. Here \mathbf{b} is also known as the chiral shift [73, 4], \mathbf{k} denotes the wavevector, v_F denotes the Fermi velocity, $\boldsymbol{\sigma}$ is the vector of Pauli matrices, and I is the 2×2 identity matrix.



From Eq. (4), the band dispersion is determined as

$$E_{\lambda}(\mathbf{k}) = -\lambda\hbar b_0 \pm \hbar v_F |\mathbf{k} + \lambda\mathbf{b}|, \quad (5)$$

where $\lambda = \pm 1$ is the node's chirality. Fig. 3 shows the scheme of band dispersion in the cases (a) $\mathbf{b} \neq \mathbf{0}$ and $b_0 \neq 0$ and (b) $\mathbf{b} = \mathbf{0}$ and $b_0 = 0$. The latter case, where the two Weyl nodes coalesce, is referred to as a Dirac semimetal.

We make a few remarks. First, the model is paradigmatic and highlights the two hallmark properties of Weyl semimetals: linear dispersion and chiral Weyl nodes. Second, the model suffices to describe the universal low-energy phenomena in Weyl semimetals. It can be shown by explicit calculation that the general properties do not change if one uses a more realistic periodic two-band model [74, 4]. Third, nonzero \mathbf{b} and b_0 require the breaking of time-reversal and parity-inversion symmetries, respectively. Fourth, we note that the opposite sign convention of \mathbf{b} and b_0 has been used in some works [4]. Finally, we note that the ideal magnetic Weyl semimetal with the minimum number of Weyl points may be realized in real materials such as $\text{K}_2\text{Mn}_3(\text{AsO}_4)_3$ [75], or EuCd_2As_2 subjected to an external magnetic field [76].

2.2 Axion electrodynamics

To characterize the electromagnetic properties of the Weyl semimetal as described by Eq. (4), we first briefly review the Lagrangian approach to Maxwell's equa-

tions [77]. We start with the conventional Maxwell Lagrangian density:

$$\mathcal{L}_0(\mathbf{r}, t) = \frac{\epsilon_0}{2} \mathbf{E}^2 - \frac{1}{2\mu_0} \mathbf{B}^2 - \rho\phi + \mathbf{J} \cdot \mathbf{A}. \quad (6)$$

Here, the potentials $\phi(\mathbf{r}, t)$ and $\mathbf{A}(\mathbf{r}, t)$ are the independent variables; the electric field $\mathbf{E}(\mathbf{r}, t)$ and the magnetic field $\mathbf{B}(\mathbf{r}, t)$ are expressed in terms of potentials:

$$\mathbf{B} = \nabla \times \mathbf{A}, \quad \mathbf{E} = -\nabla\phi - \frac{\partial \mathbf{A}}{\partial t}. \quad (7)$$

Equations (7) already imply two of the four Maxwell's equations:

$$\nabla \cdot \mathbf{B} = 0, \quad \nabla \times \mathbf{E} + \frac{\partial \mathbf{B}}{\partial t} = 0. \quad (8)$$

We define the action

$$S_0 = \int dt d^3\mathbf{r} \mathcal{L}_0(\mathbf{r}, t), \quad (9)$$

and require S_0 to be stationary with respect to the variations of $\phi(\mathbf{r}, t)$ and $\mathbf{A}(\mathbf{r}, t)$.

Then we obtain the other two of the four Maxwell's equations:

$$\nabla \cdot \mathbf{E} = \frac{\rho}{\epsilon_0}, \quad \nabla \times \mathbf{B} = \mu_0 \mathbf{J} + \frac{1}{c^2} \frac{\partial \mathbf{E}}{\partial t}. \quad (10)$$

See Ref. [77, §24] for detailed derivation of Eq. (10).

Now, we introduce the formalism of axion electrodynamics [78]. Axion electrodynamics was first proposed in high-energy physics to solve the strong CP problem in quantum chromodynamics [79]. In condensed matter physics, axion electrodynamics is used to understand the properties of ^3He [80], topological insulators [81, 82, 83, 68], and Weyl semimetals [74, 84, 85, 86]. For Weyl semimetals, axion electrodynamics describes the topological effects of Weyl node separation. The usage of axion electrodynamics in Weyl semimetals will be discussed in the next subsection.

Axion electrodynamics is generated by adding to Eq. (6) an additional term (the θ term) [78, 87]:

$$\mathcal{L}_\theta = 2\alpha \sqrt{\frac{\epsilon_0}{\mu_0}} \frac{\theta}{2\pi} \mathbf{E} \cdot \mathbf{B}, \quad (11)$$

where $\alpha = \frac{e^2}{4\pi\epsilon_0\hbar c}$ is the fine structure constant, and $\theta(\mathbf{r}, t)$ is a pseudoscalar field.

Now

$$S = \int dt d^3\mathbf{r} [\mathcal{L}_0(\mathbf{r}, t) + \mathcal{L}_\theta(\mathbf{r}, t)]. \quad (12)$$

This does not modify Eqs. (8), but changes Eqs. (10) into (see Ref. [88] for detailed derivation):

$$\nabla \cdot \mathbf{E} = \frac{\rho}{\epsilon_0} - 2c\alpha \nabla \left(\frac{\theta}{2\pi} \right) \cdot \mathbf{B}, \quad (13)$$

$$\nabla \times \mathbf{B} = \mu_0 \mathbf{J} + \frac{1}{c^2} \frac{\partial \mathbf{E}}{\partial t} + \frac{2\alpha}{c} \left[\frac{\partial}{\partial t} \left(\frac{\theta}{2\pi} \right) \mathbf{B} + \nabla \left(\frac{\theta}{2\pi} \right) \times \mathbf{E} \right]. \quad (14)$$

These modified Maxwell's equations contain most (although not all) of the new physics of axion electrodynamics [89]. Here we note that the θ term enters the equations only through derivatives. This is as expected since if θ is constant [90], the θ term is a total derivative and irrelevant for the equation of motion.

There is a different yet equivalent way to describe axion electrodynamics [90], where one keeps the macroscopic Maxwell's equations in their original form:

$$\nabla \cdot \mathbf{B} = 0, \quad \nabla \times \mathbf{E} = -\frac{\partial \mathbf{B}}{\partial t}, \quad (15)$$

$$\nabla \cdot \mathbf{D} = \rho, \quad \nabla \times \mathbf{H} = \mathbf{J} + \frac{\partial \mathbf{D}}{\partial t}, \quad (16)$$

with the modified constitutive relations:

$$\mathbf{D} = \epsilon_0 \mathbf{E} + 2\alpha c \epsilon_0 \frac{\theta}{2\pi} \mathbf{B}, \quad \mathbf{H} = \frac{1}{\mu_0} \mathbf{B} - 2\alpha \frac{1}{c\mu_0} \frac{\theta}{2\pi} \mathbf{E}. \quad (17)$$

There is yet another way to describe axion electrodynamics if $\theta(\mathbf{r}, t)$ satisfies the additional condition:

$$\nabla \left[\frac{\partial \theta}{\partial t}(\mathbf{r}, t) \right] = \mathbf{0}. \quad (18)$$

Then one can express Maxwell's macroscopic equations in the frequency domain:

$$\nabla \cdot \mathbf{B} = 0, \quad \nabla \times \mathbf{E} = i\omega \mathbf{B}, \quad (19)$$

$$\nabla \cdot \mathbf{D} = \rho, \quad \nabla \times \mathbf{H} = \mathbf{J} - i\omega \mathbf{D}. \quad (20)$$

with the constitutive relation [91]:

$$\mathbf{D} = \varepsilon_0 \mathbf{E} + 2\alpha c \varepsilon_0 \frac{1}{-i\omega} \left[\frac{\partial}{\partial t} \left(\frac{\theta}{2\pi} \right) \mathbf{B} + \nabla \left(\frac{\theta}{2\pi} \right) \times \mathbf{E} \right], \quad \mathbf{H} = \frac{1}{\mu_0} \mathbf{B}. \quad (21)$$

Such a description is equivalent to the previous two under the assumption of Eq. (18). It will be useful later when we discuss Weyl semimetals.

2.3 The axion term

It is known that the effects of Weyl node separation are fully described by an axion term

$$\theta(r, t) = 2\mathbf{b} \cdot \mathbf{r} - 2b_0 t. \quad (22)$$

Substituting Eq. (22) into Eq. (21) and replacing ε_0 with $\varepsilon_D(\omega)$, we obtain Eq. (3). (Note that Eq. (22) satisfies the assumption of Eq. (18).)

The above result is standard; its derivation is beyond the scope of this tutorial. We only note that the derivation uses Fujikawa's method in the fermion path integral formulation; the θ term corresponds to the chiral anomaly, a type of quantum anomalies that arises from a nontrivial Jacobian in the change of path integral variables. We refer readers to Ref. [74] for the original derivation of Eq. (22), Ref. [92] for fermion path integrals, and Ref. [93] for quantum anomalies and Fujikawa's method.

2.4 The Dirac term

Now we derive the Dirac term $\varepsilon_D(\omega)$ in Eq. (3), i.e., the permittivity of a Dirac semimetal (Fig. 3b). The Dirac semimetal can be described by a simple two-band Hamiltonian:

$$H_D = \hbar v_F \mathbf{k} \cdot \boldsymbol{\sigma}, \quad (23)$$

while the spin degeneracy is taken into account by a degeneracy factor $g = 2$.

From the Hamiltonian Eq. (23), we obtain the low-energy spectra:

$$E_{\mathbf{k},s} = s\hbar v_F |\mathbf{k}|, \quad (24)$$

where $s = \pm 1$ denote the band indices. The eigenstates are:

$$|\mathbf{k}, +\rangle = \begin{pmatrix} \cos \frac{\vartheta}{2} \\ e^{i\varphi} \sin \frac{\vartheta}{2} \end{pmatrix}, \quad |\mathbf{k}, -\rangle = \begin{pmatrix} -\sin \frac{\vartheta}{2} \\ e^{i\varphi} \cos \frac{\vartheta}{2} \end{pmatrix}, \quad (25)$$

where ϑ and φ are respectively the polar and azimuthal angles of the three-dimensional \mathbf{k} .

Then $\varepsilon_D(\omega)$ can be determined by the standard linear response theory [94, 95]:

$$\varepsilon_D(\omega) = \varepsilon_b + i \frac{\sigma(\omega)}{\omega}, \quad (26)$$

where ε_b is the background permittivity due to the other bands and $\sigma(\omega)$ is the dynamic conductivity tensor due to the Dirac cone. Assuming noninteracting electrons and local response, $\sigma(\omega)$ is given by Kubo-Greenwood formula [96, 6]:

$$\sigma_{\alpha\beta}(\omega) = \frac{-ie^2 g \hbar}{V} \sum_{\mathbf{k}, s, s'} \frac{n(E_{\mathbf{k}, s}) - n(E_{\mathbf{k}, s'})}{E_{\mathbf{k}, s} - E_{\mathbf{k}, s'}} \frac{\langle \mathbf{k} s | \hat{v}_\alpha | \mathbf{k} s' \rangle \langle \mathbf{k} s' | \hat{v}_\beta | \mathbf{k} s \rangle}{\hbar(\omega + i0) + E_{\mathbf{k}, s} - E_{\mathbf{k}, s'}}. \quad (27)$$

Here $\alpha, \beta = x, y, z$, ω is the incident light frequency, V is the volume, $\hat{v}_\alpha = \frac{1}{\hbar} \frac{\partial H_D}{\partial k_\alpha} = v_F \sigma_\alpha$ is the velocity operator, $|\mathbf{k} s\rangle$ and $|\mathbf{k} s'\rangle$ are the initial and final electronic state, and

$$n(E) = \frac{1}{e^{(E-E_F)/k_B T} + 1} \quad (28)$$

is the Fermi distribution where E_F is the Fermi energy and T is the temperature.

Since the Hamiltonian Eq. (23) is isotropic in \mathbf{k} , the conductivity tensor $\sigma(\omega)$ is also isotropic and can be treated as a scalar. Detailed calculation shows [6]:

$$\sigma(\omega) = \frac{e^2 g k_F}{\hbar 24\pi} \Omega \tilde{G}(\Omega/2) + i \frac{e^2 g k_F}{\hbar 24\pi^2} \left\{ \frac{4}{\Omega} \left[1 + \frac{\pi^2}{3} \left(\frac{k_B T}{E_F} \right)^2 \right] + 8\Omega \int_0^{\varepsilon_c} \frac{\tilde{G}(\varepsilon) - \tilde{G}(\Omega/2)}{\Omega^2 - 4\varepsilon^2} \varepsilon d\varepsilon \right\}, \quad (29)$$

where $k_F = E_F/\hbar v_F$, $\Omega = \hbar(\omega + i\tau^{-1})/E_F$, τ^{-1} is the Drude damping rate, $\varepsilon_c = E_c/E_F$, and E_c is the cutoff energy beyond which the band dispersion is no longer linear. Moreover, the function $\tilde{G}(x)$ in Eq. (29) reads:

$$\tilde{G}(x) \equiv n(-xE_F) - n(xE_F) = \frac{\sinh(xE_F/k_B T)}{\cosh(E_F/k_B T) + \cosh(xE_F/k_B T)}. \quad (30)$$

The physical meaning of Eq. (29) is more transparent in the low-temperature limit when $k_B T \ll E_F$. Then $\tilde{G}(\Omega/2) \rightarrow \Theta(\Omega - 2)$ where $\Theta(\cdot)$ is the Heaviside step function, and thus:

$$\sigma(\omega) = \frac{e^2 g k_F}{\hbar 24\pi} \Omega \Theta(\Omega - 2) + i \frac{e^2 g k_F}{\hbar 24\pi^2} \left[\frac{4}{\Omega} - \Omega \ln \frac{4\varepsilon_c^2}{|\Omega^2 - 4|} \right] \quad (31)$$

For the real part of $\sigma(\omega)$, the step function captures the interband absorption when $E > 2E_F$. For its imaginary part, the first term is the Drude term due to the intraband transition, while the second term is the correction due to the interband transitions.

2.5 Giant optical nonreciprocity

Now we can discuss one unique property of magnetic Weyl semimetals: giant optical nonreciprocity without an external magnetic field. Reciprocity is a fundamental internal symmetry of Maxwell's equations [97, 98, 99, 100, 101]. It imposes direct constraints on basic optical phenomena including transmission [102], reflection [103], absorption, and emission [104, 105]. Conversely, breaking reciprocity enables significant new opportunities in photonic applications such as isolation [106, 107], circulation [108], robust topological transport [109, 110], and violation of Kirchhoff's law of thermal radiation [111, 112].

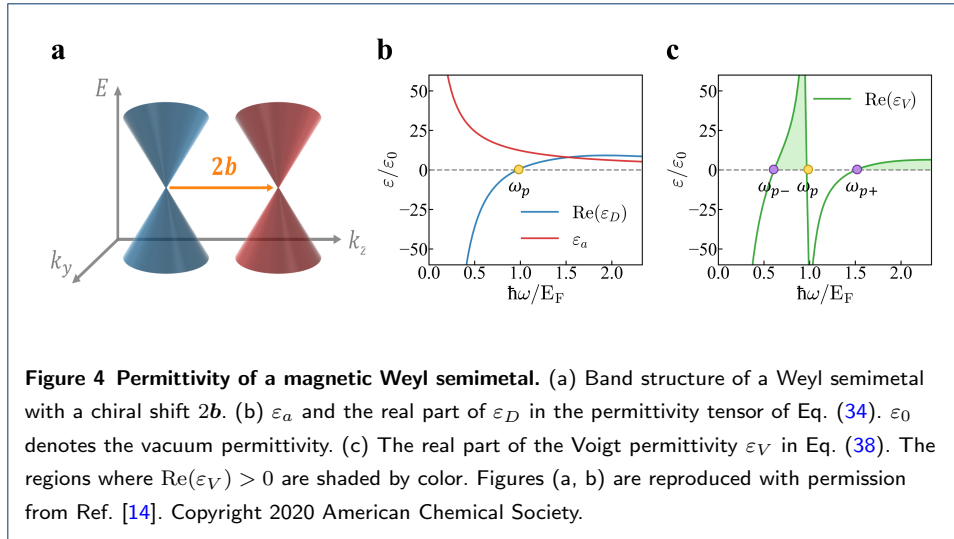
Optical materials with significant nonreciprocal responses are rare. The most used ones are magneto-optical materials [113]. Under an external magnetic field, this type of material has an asymmetric dielectric tensor $\varepsilon \neq \varepsilon^T$ that breaks reciprocity (ε^T denotes the transpose of ε). The strength of nonreciprocal effects depends on the degree of asymmetry of ε [113]:

$$\gamma = \frac{\|\varepsilon - \varepsilon^T\|}{\|\varepsilon + \varepsilon^T\|}, \quad (32)$$

where $\|\cdot\|$ denotes the matrix norm. For magneto-optical materials,

$$\gamma \sim \frac{\omega_c}{\omega}, \quad (33)$$

where ω is the light frequency, $\omega_c = eB/m^*$ is the cyclotron frequency, m^* is the effective electron mass, e is the electron charge, and B is the external magnetic field [113, 111]. For the typical magnetic field $B \sim 1$ T, $\omega_c \sim 1$ THz, thus $\gamma \sim 0.001$ -



0.01 at optical frequencies. Therefore, the nonreciprocal effect is weak in magneto-optical materials.

In contrast, magnetic Weyl semimetals can exhibit extremely large nonreciprocal responses, with $\gamma \sim 1$ at optical frequencies. As an illustration, we consider a Weyl semimetal with \mathbf{b} along the z -direction and $b_0 = 0$ (Fig. 4a). It has a permittivity tensor:

$$\varepsilon(\omega) = \begin{pmatrix} \varepsilon_D & i\varepsilon_a & 0 \\ -i\varepsilon_a & \varepsilon_D & 0 \\ 0 & 0 & \varepsilon_D \end{pmatrix}, \quad (34)$$

where $\varepsilon_D(\omega)$ is given by Eqs. (26) and (29), and

$$\varepsilon_a(\omega) = \frac{be^2}{2\pi^2\hbar\omega}. \quad (35)$$

The permittivity tensor $\varepsilon(\omega)$ has the typical form of a gyrotropic medium [113]. Following Ref. [6], we use the parameters $\varepsilon_b/\varepsilon_0 = 6.2$, $\xi_c = 3$, $g = 2$, $\tau = 1000$ fs, $b = 2 \times 10^9$ /m, $v_F = 0.83 \times 10^5$ m/s, $T = 300$ K, and $E_F = 0.15$ eV. Fig. 4b plots the calculated ε_D and ε_a . The magnitude of ε_a is comparable to ε_D over a broad frequency range. Hence $\gamma \sim |\varepsilon_a/\varepsilon_D| \sim 1$. Such a strong nonreciprocity originates from the anomalous Hall effect induced by the Weyl node separation [2, 4, 114]. This mechanism is fundamentally different from the cyclotron mechanism for magneto-optical materials. In particular, it requires no external magnetic field.

2.6 Electromagnetic waves in the bulk medium

The strong gyrotropy significantly affects the behavior of light in magnetic Weyl semimetals. As the first example, we study the electromagnetic waves in the bulk medium as described by $\varepsilon(\omega)$ in Eq. (34). The results will be useful later in discussing many applications.

We consider the Voigt configuration, i.e., the wavevector \mathbf{k} is in the plane perpendicular to the axis of gyration \mathbf{b} . Such a configuration is mirror symmetric with respect to that plane, thus waves can be decoupled into TE and TM modes [115]. TE/TM modes have the electric/magnetic fields parallel to \mathbf{b} ; their dispersion relations can be expressed as:

$$\text{TE:} \quad k^2 = \omega^2 \mu_0 \varepsilon_D(\omega), \quad (36)$$

$$\text{TM:} \quad k^2 = \omega^2 \mu_0 \varepsilon_V(\omega). \quad (37)$$

where we have introduced the Voigt permittivity for TM modes as:

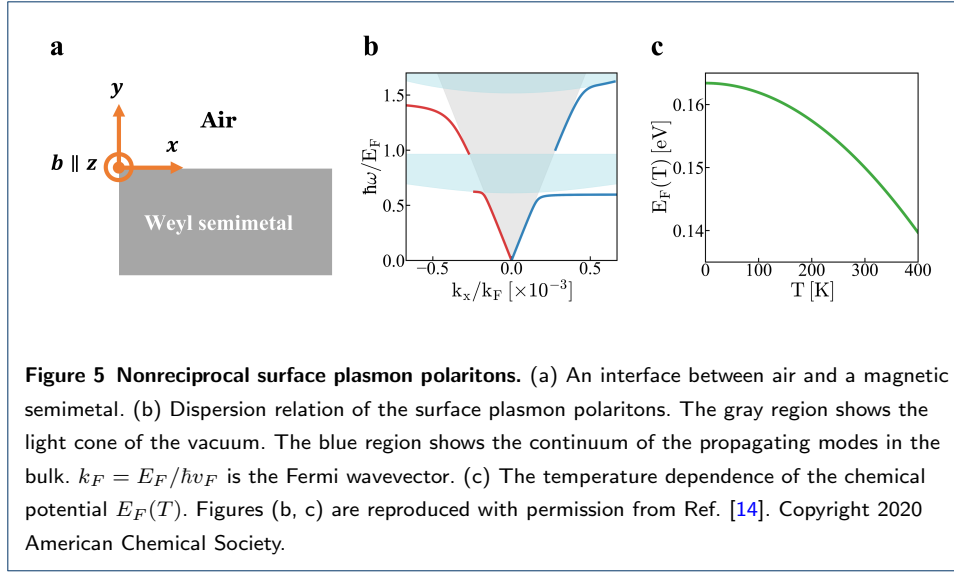
$$\varepsilon_V(\omega) = \varepsilon_D - \frac{\varepsilon_a^2}{\varepsilon_D}. \quad (38)$$

Fig. 4c plots the calculated $\varepsilon_V(\omega)$ with the parameters as described in Sec. 2.5.

We note that the gyrotropic medium behaves differently for the two modes due to the different permittivity components: ε_D for TE modes in Eq. (36) and ε_V for TM modes in Eq. (37). Moreover, the two permittivities have different frequency dependence. For TE modes, ε_D is not affected by the gyrotropy (Fig. 4b). It monotonically increases with the frequency and has a plasma frequency ω_p . For TM modes, ε_V is affected by the gyrotropy (Fig. 4c). The existence of the chiral shift $2\mathbf{b}$ splits ε_V into two branches which are separated by ω_p . In each branch, ε_V monotonically increases with the frequency and has an effective plasma frequency ω_{p-} and ω_{p+} , respectively. Consequently, when $\omega_{p-} < \omega < \omega_p$, $\text{Re}(\varepsilon_D)$ is negative while $\text{Re}(\varepsilon_V)$ is positive; when $\omega_p < \omega < \omega_{p+}$, $\text{Re}(\varepsilon_D)$ is positive while $\text{Re}(\varepsilon_V)$ is negative.

2.7 Nonreciprocal surface plasmon polaritons

As the second example, we study the surface plasmon polaritons of a Weyl semimetal [91]. The results will also be useful for later applications.



We consider a planar interface between air and a semi-infinite magnetic Weyl semimetal with a chiral shift $2\mathbf{b}$ along the z direction parallel to the interface (Fig. 5a). Such an interface supports nonreciprocal surface plasmon polaritons, whose band dispersion along the x direction is determined by: [6, 116]

$$k_y + \varepsilon_V k_{y0} - k_x \frac{\varepsilon_a}{\varepsilon_D} = 0, \quad (39)$$

where $k_0(\omega) = \omega/c$ is the wavenumber in vacuum, k_x is the x -component of the wavevector, $k_{y0} = \sqrt{k_x^2 - k_0^2}$ and $k_y = \sqrt{k_x^2 - \varepsilon_V k_0^2}$ are the y -component of the wavevector in air and in the Weyl semimetal, respectively. The last term in Eq. (39) shows that when the sign of k_x flips, the frequency of the surface plasmon polaritons will be different, i.e., $\omega(k_x) \neq \omega(-k_x)$. The asymmetry of the dispersion is induced by the gyrotropy; it occurs only when $\varepsilon_a \neq 0$.

Fig. 5b shows the calculated band dispersion of the surface plasmon polaritons, together with the continuum region of bulk modes (in light blue) and the light cone of vacuum (in light gray). We note that the surface plasmon polaritons approximately occupy the frequency ranges $\omega < \omega_{p-}$ and $\omega_p < \omega < \omega_{p+}$; the bulk modes occupy the frequency ranges $\omega_{p-} < \omega < \omega_p$ and $\omega > \omega_{p+}$. This is as expected from the frequency dependence of ε_V in Fig. 4c. The dispersion of the surface plasmon polaritons is clearly asymmetric near the effective plasma frequencies ω_{p-} and ω_{p+} . Away from the effective plasma frequencies, the dispersion becomes approximately symmetric. The frequency range where the dispersion is evidently asymmetric mea-

sures the strength of nonreciprocity. The plots confirm the strong nonreciprocity of a magnetic Weyl semimetal without an external magnetic field. As a comparison, to obtain a similar strength of nonreciprocity, conventional magneto-optical materials, such as InSb, need an unrealistically large external magnetic field of about 100 T [14, 7]. This is consistent with our order-of-magnitude comparison of γ in Sec. 2.5.

2.8 Tunable Fermi level

Another unique property of Weyl semimetals is the large tunability of the Fermi level E_F (also referred to as the chemical potential). The variation of the Fermi level can significantly affect the optical conductivity according to Eq. (29). This leads to greatly tunable optical phenomena. The Fermi level of a Weyl semimetal can be adjusted in different ways. Below we discuss two approaches.

First, the Fermi level can be tuned by electric gating. This is because an undoped Weyl semimetal features a vanishing density of states at the energy of Weyl points. Therefore, the carrier concentrations are much lower than metals and thus are more easily depleted. Second, the Fermi level can be tuned by thermal tuning. This is because a Weyl semimetal has a small and nonconstant density of states and a linear dispersion. Consequently, its Fermi level is strongly temperature dependent. The Fermi level as a function of temperature can be calculated from the requirement of charge conservation [117]:

$$E_F(T) = \frac{2^{1/3} \left(9E_F(0)^3 + \sqrt{81E_F(0)^6 + 12\pi^6 k_B^6 T^6} \right)^{2/3} - 2\pi^2 3^{1/3} k_B^2 T^2}{6^{2/3} \left(9E_F(0)^3 + \sqrt{81E_F(0)^6 + 12\pi^6 k_B^6 T^6} \right)^{1/3}}. \quad (40)$$

Fig. 5c shows $E_F(T)$, where we set $E_F(0) = 0.163$ eV such that $E_F(300\text{K}) = 0.150$ eV. Note that $E_F(T)$ decreases as T increases. Consequently, the dielectric tensor and optical properties of the Weyl semimetal are also temperature dependent.

2.9 Effects of Fermi arcs

As we mentioned in Sec. 1.2, Weyl semimetals feature not only Weyl nodes in the bulk band structure but also Fermi arc surface states. The existence of Fermi arc surface states can modify the boundary conditions of Maxwell's equations, which can affect the optical properties of Weyl semimetals. Depending on the problems,

the modification may be negligible in some cases but may be significant in other cases.

So far, we have focused on the optical effects that arise from the nontrivial *bulk* electronic states in Weyl semimetals. Now we point to some works that highlight the optical effects of Fermi arcs. Ref. [118] provides a semiclassical approach to understanding surface Fermi arcs in Weyl semimetals. Ref. [119] provides a detailed calculation of optical properties of Weyl semimetals including the effects of both bulk states and Fermi arc surface states, and compares their contributions to bulk and surface conductivity tensors. Refs. [120, 121] study “Fermi arc plasmons” that originate from the hybridization of collective modes associated with Fermi arc carriers and bulk carriers. Such an unusual surface plasmon mode exhibits a hyperbolic band dispersion [122]. Ref. [123] systematically studies both the bulk plasmons and the Fermi-arc plasmons over opposite surfaces of a Weyl semimetal slab.

3 Photonic applications and devices

In this section, we survey various photonic applications of Weyl semimetals. These applications utilize nontrivial linear and nonlinear optical effects of Weyl semimetals. For each application, we discuss both the physical mechanism and the device configuration.

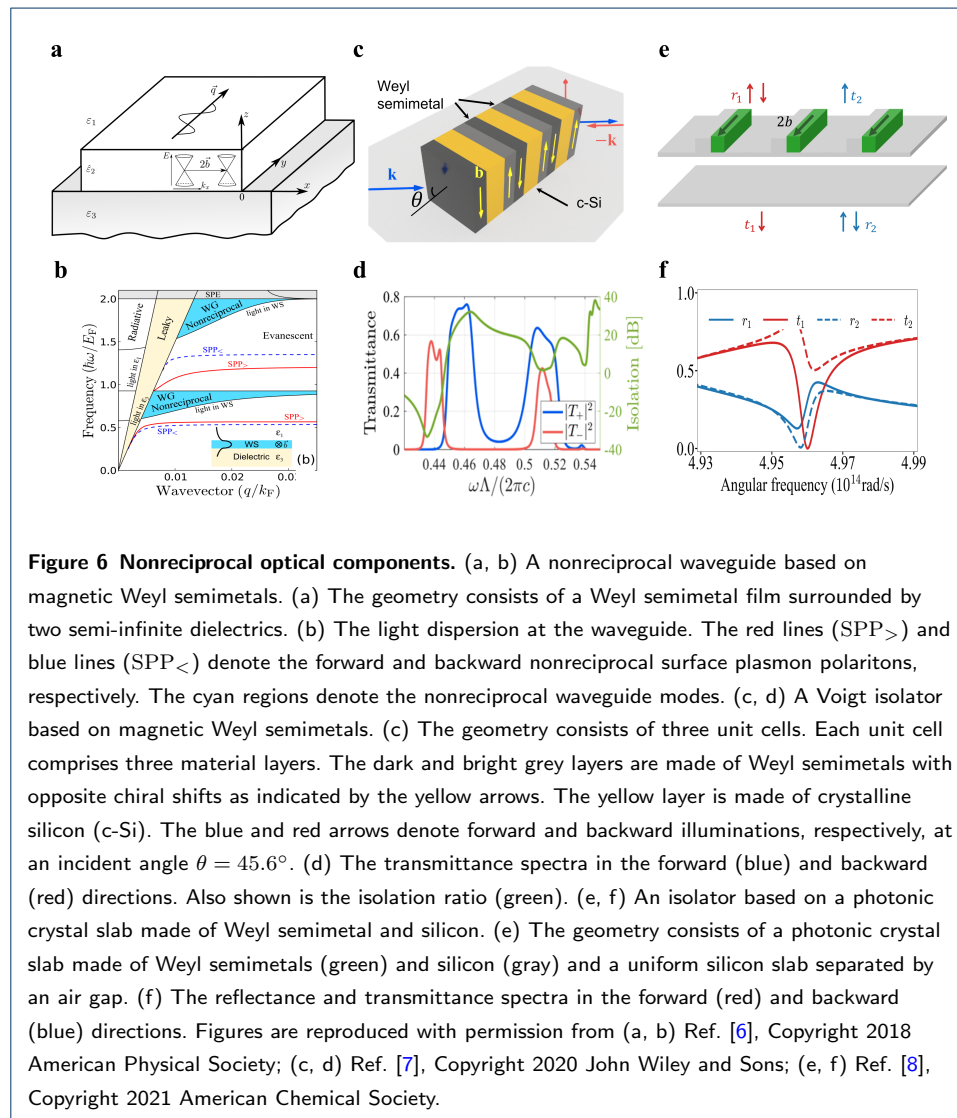
3.1 Linear optical effects

3.1.1 Nonreciprocal optical components

Nonreciprocal optical components, such as isolators [107], circulators [124], and nonreciprocal waveguides, are crucial in many photonic applications including optical circuits [125, 126], and lasers [127]. As we discussed in Sec. 2.5, magnetic Weyl semimetals can exhibit giant optical nonreciprocity without an external magnetic field [91, 6] thanks to the anomalous Hall effect [72, 128, 76, 43, 42, 44]. Hence, magnetic Weyl semimetals can be used to construct efficient and compact nonreciprocal optical components. Here, we review three examples of nonreciprocal optical components based on magnetic Weyl semimetals.

In Ref. [6], Kotov et al. design a nonreciprocal waveguide using magnetic Weyl semimetals. As shown in Fig. 6a, the structure consists of a Weyl semimetal thin film sandwiched by two dielectrics. The chiral shift $2\mathbf{b}$ is along the x direction. Fig. 6b shows the dispersion diagram of the TM-polarized light propagating in the

y direction. The structure supports two different types of guided modes depending on the light frequency ω : When $\omega < \omega_{p-}$ or $\omega_p < \omega < \omega_{p+}$, the structure supports nonreciprocal surface plasmon polaritons; when $\omega_{p-} < \omega < \omega_p$ or $\omega > \omega_{p+}$, the structure supports nonreciprocal waveguide modes. Such behavior is similar to that shown in Fig. 5b and is as expected from the frequency dependency of ε_V in Fig. 4c. The dispersions of these guided modes can be tuned via gating between the THz and mid-IR ranges.



In Ref. [7], Asadchy et al. design optical isolators in the mid-IR range using magnetic Weyl semimetals, with both Faraday and Voigt geometries. The Faraday isolator consists of a Weyl semimetal slab sandwiched by two twisted polarization

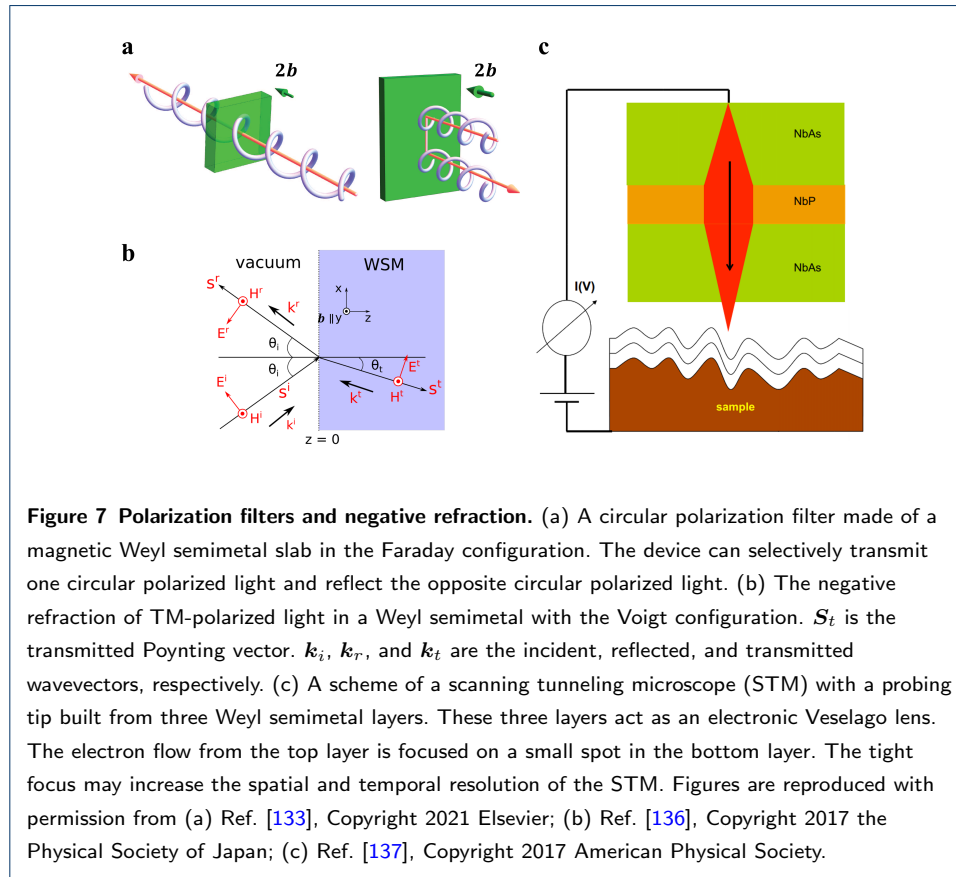
filters and operates at the normal incidence. The chiral shift $2b$ is along the direction perpendicular to the slab. The Voigt isolator (Fig. 6c) is a finite one-dimensional photonic crystal with a three-layer unit cell consisting of Weyl semimetal, dielectric, and Weyl semimetal; the chiral shifts of the two Weyl semimetal layers are both parallel to the slab but in the opposite directions. Such a structure is designed for optical isolation at oblique incidence. It breaks all the symmetries that preclude isolation [129]. Numerical results show that three unit cells suffice to achieve high isolation and low insertion loss. Remarkably, the total thickness of the device is less than 1.4 times the operation wavelengths, and is three orders of magnitude smaller than that of conventional isolators based on magneto-optical materials. Fig. 6d shows the calculated power transmittance spectra in the forward and backward directions at the incident angle of $\theta = 45.6^\circ$. The two spectra are significantly different. Near the resonance frequency, the device achieves greater than 30 dB isolation and less than 1.2 dB insertion loss. In Ref. [130], Li et al. demonstrate a similar isolation performance using a one-dimensional photonic crystal containing a defect layer made of magnetic Weyl semimetals.

In Ref. [8], Park et al. design a photonic crystal slab structure made of magnetic Weyl semimetal and silicon, which can achieve optical isolation at normal incidence without the need for polarizers. As shown in Fig. 6e, the structure consists of a photonic crystal slab and a uniform dielectric slab separated by an air gap. The total thickness of the device is less than the operational wavelength. Such a structure hosts guided resonances [131] that can greatly enhance the nonreciprocal effects. Fig. 6f shows the calculated power transmission and reflection spectra for the TM polarized light in the forward and backward directions. The spectra exhibit high contrast near the guided resonance.

3.1.2 Polarization filters

Due to the giant gyrotropy of magnetic Weyl semimetals, the left and right circularly polarized light propagating along the chiral shift direction will acquire different phases and attenuation [132]. Such effects can be used to construct polarization filters. In Ref. [133], Chitchekatchev et al. demonstrate that a single magnetic Weyl semimetal slab can selectively transmit/reflect circularly polarized light in the Faraday configuration, and linearly polarized light in the Voigt configuration (Fig. 7a).

In Ref. [134], Yang et al. design a circular polarizer using two layers of magnetic Weyl semimetals separated by an air gap. The chiral shifts of the two Weyl semimetals are parallel and perpendicular to the slab. The proposed device exhibits a high circular polarization efficiency and high average transmittance in the wavelength region from $9\ \mu\text{m}$ to $15\ \mu\text{m}$ at incidence angles up to 50° . In Ref. [135], Mukherjee et al. study the effect of a tilt of the Weyl cones on the absorption of left and right circular polarized light. They show that the difference in absorption depends strongly on the degree of tilt.



3.1.3 Negative refraction

Negative refraction refers to the counter-intuitive phenomenon where light is refracted at a negative angle with respect to the surface normal [138]. Negative refraction is related to exotic phenomena such as perfect lensing [139]. There are several known routes to achieving negative refraction. The original approach proposed by Veselago [138] requires the use of a negative index material where both the permittivity and the permeability are negative. Such “double-negative” materials

have been experimentally demonstrated by metamaterials [140]. Negative refraction has also been achieved in photonic crystals [141, 142, 143]. Another approach utilizes the magnetoelectric effect in chiral media [144, 145, 146], which has also been experimentally confirmed using chiral metamaterials [147].

Weyl semimetals can provide a new route to negative refraction using natural materials. As we discussed in Sec. 2.6, TM-polarized light can propagate in a magnetic Weyl semimetal with the Voigt configuration when $\omega_{p-} < \omega < \omega_p$ or $\omega > \omega_{p+}$. In the lower frequency range, the light can propagate in the bulk below the plasma frequency ω_p . This phenomenon is typical for any gyrotropic system in the Voigt configuration [115, 6] and is related to the modification of ε_V by the gyrotropy as shown in Fig. 4c. Interestingly, this phenomenon is also accompanied by negative refraction. In Refs. [136, 148], it is shown that TM-polarized light in the lower frequency range propagates with opposite signs of phase and group velocities. Hence the light exhibits a negative refractive index (Fig. 7b). Although such negative refraction can be observed in any gyrotropic media, magnetic Weyl semimetals can exhibit the phenomena over a much broader bandwidth without any external magnetic field. These predictions still await experimental confirmation.

Although not the focus of this paper, we point out that similar negative refraction for *electrons* can also occur in a Weyl semimetal [137, 149]. The phenomenon of negative refraction for electrons is similar to that for photons, although the physical mechanisms are different. Such an effect can be used to construct a three-dimensional electronic Veselago lens. In Ref. [137], Hills et al. design an electronic Veselago lens made of three layers of different Weyl semimetals. They propose to use such a lens as a probing tip for scanning tunneling microscope (STM) to significantly improve its spatial and temporal resolution (Fig. 7c). In Ref. [149], Tchoumakov et al. design a three-dimensional electronic Veselago lens made of a single Weyl semimetal. Such a Veselago lens is based on chiral anomaly and can selectively focus electrons of a given chirality.

3.2 Nonlinear optical effects

So far, we have only discussed the linear optical effects of Weyl semimetals. These phenomena can be understood in the context of linear response theory [94, 150], as we have demonstrated in Sec. 2. Weyl semimetals can also exhibit pronounced

nonlinear optical effects [151]. These phenomena must be understood in the context of nonlinear response theory [152]. Nonlinear responses of topological materials have only been investigated recently [153, 154, 155, 156, 157, 11, 158, 159, 160, 161]; a systematic discussion is beyond the scope of this paper. Instead, we survey some nonlinear optical effects and applications of Weyl semimetals.

3.2.1 Photogalvanic effect

One of the simplest nonlinear optical effects in a solid is the photogalvanic effect. It refers to the generation of the direct current (DC) in the crystal under exposure to light. In the context of nonlinear optics [162], the photogalvanic effect is a second-order nonlinear optical effect: A direct current can appear in a *noncentrosymmetric* solid due to an oscillating electric field when one analyzes the response up to (at least) second order in the applied field [163]. At this order of perturbation theory, the DC photocurrents \mathbf{J} are the sum of three contributions [164, 165]:

$$\mathbf{J} = \mathbf{J}_{\text{injection}} + \mathbf{J}_{\text{shift}} + \mathbf{J}_{\text{anomalous}}, \quad (41)$$

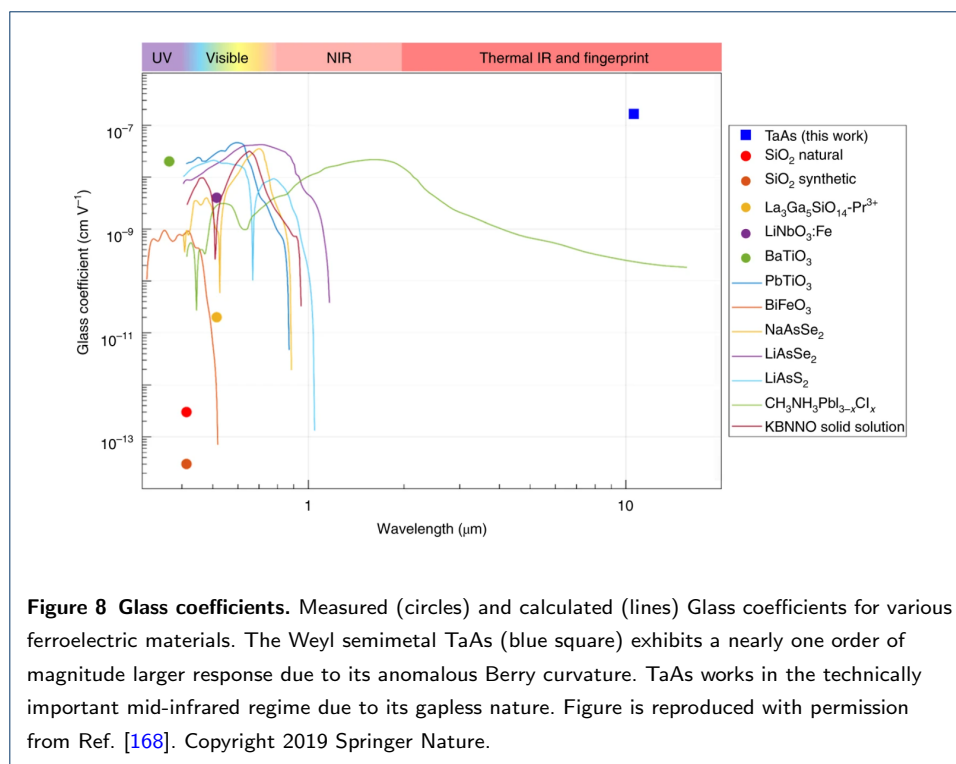
where the three terms are referred to as “injection”, “shift”, and “anomalous” current contributions in the literature. These three contributions have different physical origins and symmetry requirements. Moreover, they exhibit different dependence on scattering time: $\mathbf{J}_{\text{injection}}$ is proportional to the scattering time τ , while $\mathbf{J}_{\text{shift}}$ and $\mathbf{J}_{\text{anomalous}}$ have well-defined DC values even in the absence of scattering [164]. Roughly speaking,

$$|\mathbf{J}_{\text{injection}}|/|\mathbf{J}_{\text{shift}}| \sim |\mathbf{J}_{\text{injection}}|/|\mathbf{J}_{\text{anomalous}}| \sim \omega\tau, \quad (42)$$

where ω is the light frequency [165]. Hence, the injection current dominates in the high-frequency or weak-scattering regime, while the shift or anomalous current dominates in the low-frequency or strong-scattering regime.

From a practical perspective, converting light to electricity is crucial for clean energy, imaging, communications, and chemical and biological sensing. For this purpose, the photogalvanic effect is of interest because it can potentially overcome the extrinsic limitations of conventional approaches. For example, traditional solar cells make use of the built-in electric fields in p-n junctions to generate photocurrent; however, their efficiency is bounded by the Shockley-Queisser limit due to the

constraint of detailed balance [166]. Thermoelectric devices utilize the optically induced thermal gradients to produce currents via the Seebeck effect; however, they require a careful balance of the optical, electronic, and thermal material properties. The photogalvanic effect provides an important alternative: It has an ultrafast response with fewer limitations on efficiency or maximum open-circuit voltage [167].



The photogalvanic effects were primarily observed in ferroelectric insulators and semiconductors [163]. However, in these materials, the photogalvanic effects are usually too weak to be technically relevant. Moreover, the photogalvanic effects are typically restricted to a narrow range of light wavelengths. For the practical usage of photogalvanic effects, it is crucial to search for materials that overcome these limitations.

Weyl semimetals can be ideal material candidates for this purpose. Recent studies show that noncentrosymmetric Weyl semimetals can exhibit a much stronger photogalvanic effect than conventional materials due to the large Berry curvature [159, 168]. The operation is broadband since Weyl semimetals exhibit zero bandgap and linear dispersion [169, 170]. Moreover, the carriers in Weyl semimetals can exhibit high mobility; the fast motion of carriers also contributes to the

ultrafast and giant photocurrent response [171]. Interestingly, Weyl semimetals exhibit topological features in all three contributions of photocurrents [155].

To compare the strength of photogalvanic effects in different materials, one calculates the so-called Glass coefficient G defined by [172, 163]:

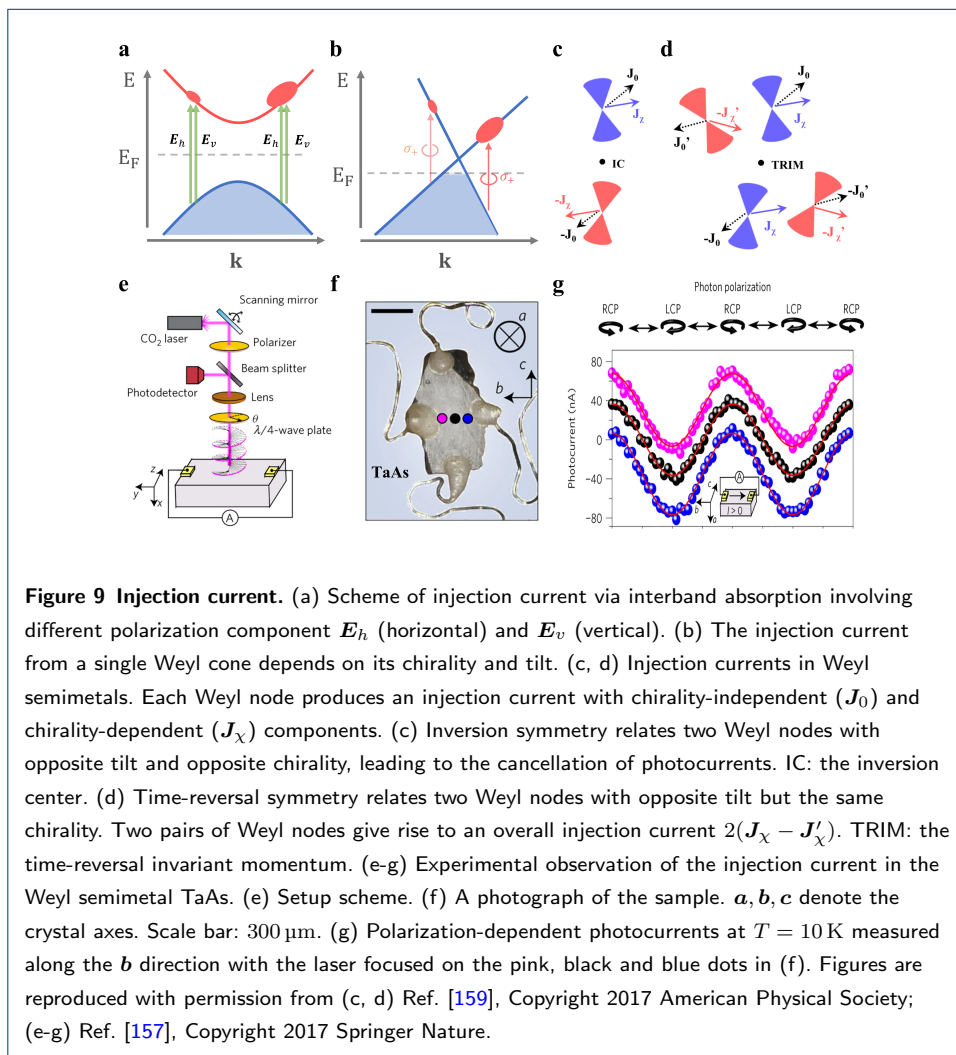
$$j = G\alpha I, \quad (43)$$

where j is the photocurrent density, α is the absorption coefficient, and I is the incident intensity. Thus G measures the generated photocurrent per absorbed power with a unit [cm/V]. Fig. 8 shows the measured and calculated Glass coefficients for various ferroelectric materials, together with the measured data for the Weyl semimetal TaAs. Notably, TaAs exhibits a nearly one order of magnitude larger response than any other materials. Moreover, TaAs enables a broadband response even in the mid-IR wavelengths, a regime that is important for thermal, chemical, and biological sensing.

Below we discuss the three contributions of photocurrents in Weyl semimetals. For each contribution, we first provide a qualitative picture of the process in general solids to explain its physical origin and symmetry requirement. Then we discuss its manifestation in Weyl semimetals. We point to relevant references for detailed quantitative analysis.

First, we discuss the injection current. Injection currents arise in a crystal that lacks certain symmetries, which give rise to phase differences between transition amplitudes associated with different polarizations of light [173]. When the crystal is excited with elliptically polarized light, the different excitation pathways for horizontal and vertical linear polarizations lead to an interference effect. This results in an asymmetric population in the wavevector space and thus generates a current (Fig. 9a). The current flips sign when the helicity of light changes sign. Because it is generated only with elliptically polarized light, the injection current is also called “circular photocurrent” [174].

The injection current requires the breaking of inversion symmetry. But this is not sufficient. Detailed symmetry analysis [164] shows that among the 21 crystal classes that lack inversion symmetry, 18 classes can support injection current; the



exceptions are $\bar{6}m2$, $\bar{6}$, and $\bar{4}3m$ [164]. For example, GaAs belongs to $\bar{4}3m$, hence cannot support injection current.

In a Weyl semimetal, the injection current can occur via asymmetric interband excitations near each Weyl cone (Fig. 9b). Each Weyl node produces an injection current that depends on its chirality and tilt, which can be decomposed as [159]:

$$\mathbf{J}^{(n)} = \mathbf{J}_0^{(n)} + \mathbf{J}_\chi^{(n)}, \quad (44)$$

where (n) denotes the n -th Weyl cone, $\mathbf{J}_0^{(n)}$ changes sign only for opposite tilts, and $\mathbf{J}_\chi^{(n)}$ changes sign only for opposite chirality. The total injection current is then the sum of contributions from all the Weyl cones.

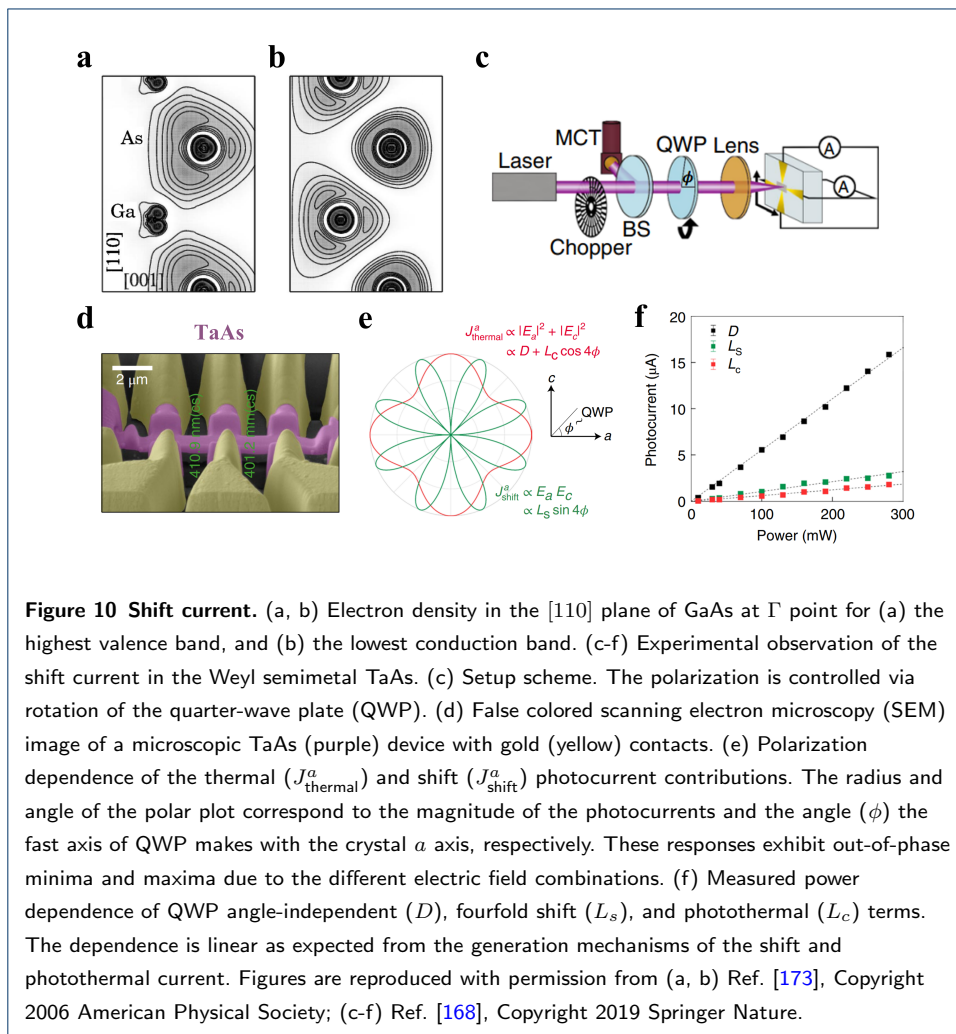
Next, we discuss the symmetry constraints. When there is inversion symmetry, a Weyl node at \mathbf{k} is related to another one at $-\mathbf{k}$ with opposite tilt and opposite chirality. When there is time-reversal symmetry, a Weyl node at \mathbf{k} is related to another one at $-\mathbf{k}$ with opposite tilt but the same chirality. Combining these symmetry considerations with Eq. (44), we conclude that in centrosymmetric Weyl semimetals, both \mathbf{J}_0 and \mathbf{J}_χ are canceled; the total injection current is zero as expected (Fig. 9c). In noncentrosymmetric Weyl semimetals with time-reversal symmetry, \mathbf{J}_0 are canceled while \mathbf{J}_χ can survive; a minimal number of two pairs of Weyl nodes can produce a nonzero response $2(\mathbf{J}_\chi - \mathbf{J}'_\chi)$ (Fig. 9d). In Weyl semimetals without any symmetry, both \mathbf{J}_0 and \mathbf{J}_χ can survive [159]. These discussions confirm the general symmetry analysis above from a different microscopic perspective.

The injection current in Weyl semimetals has been investigated both theoretically [156, 159, 158, 161, 175] and experimentally [157, 176, 177]. In Ref. [157], Ma et al. report the experimental observation of the injection current in TaAs. They use a mid-infrared scanning photocurrent microscope (Fig. 9e) equipped with a CO₂ laser with wavelength $\lambda_{\text{CO}_2} = 10.6 \mu\text{m}$ and energy $\hbar\omega = 117 \text{ meV}$. This photon energy is chosen to induce the desired interband transitions near the Weyl nodes. The TaAs sample is purposely filed down to show a clean surface with its normal direction along the \mathbf{a} ([100]) axis of the crystal (Fig. 9f). The sample is kept at a low temperature $T \approx 10 \text{ K}$ to increase the scattering time τ , which is crucial to observe the shift current [see Eq. (42)]. Light is focused and normally incident on the sample, i.e., along the \mathbf{a} axis. Its polarization is controlled by the

rotation angle θ of the quarter-wave plate. In Fig. 9g, the pink, black, and blue data points show the photocurrent along the \mathbf{b} axis when the laser is focused on the pink, black, and blue dots in Fig. 9f, respectively. When the laser is focused near the sample's center (the black dot), the photocurrent fits well to a cosine function of θ : It reaches the maximum for right circularly polarized light, the minimum for left circularly polarized light, and zero for linearly polarized light. When the laser spot is moved horizontally to the blue and pink dots, the corresponding photocurrents exhibit the same polarization dependence but with an additional, polarization-independent shift. These data reveal two distinct mechanisms for photocurrent generation. The polarization-dependent component corresponds to the injection current. The polarization-independent component arises from the photo-thermal effect [178, 179, 180]: Because the sample and contact have different thermopower, a current is generated by the laser-induced temperature gradient. Such an interpretation is further supported by additional experiments [157].

Second, we discuss the shift current. Shift currents arise from a coordinate shift accompanying the interband photoexcitation of electrons [181]. It occurs because the real-space center of charge for the valence bands differs from that for the conduction bands. As light is absorbed and electrons transit from the valence to conduction bands, there will be a motion of charge. If the crystal has low enough symmetry and the light polarization is appropriate, there will be a net current due to the “shift” of the center of charge [173]. The shift is on the order of a bondlength, and occurs on femtosecond time scales [164]. A more rigorous treatment of the shift current requires the modern theory of electric polarization [29] and the formalism of localized Wannier functions [182, 183].

As an illustration, we discuss the shift current in the intrinsic semiconductor GaAs [173]. Fig. 10a and 10b show the electron density of GaAs for the Γ electrons in the valence and conduction bands, respectively. They can be viewed as snapshots before and after the photoexcitation. Electrons at the top of the valence band (Γ point) are localized around the As atoms (Fig. 10a). During the photoexcitation, the crystal absorbs photons of energy larger than the bandgap to populate the states near the bottom of the conduction band (also Γ point). Now electrons have relocated closer to the Ga atoms (Fig. 10b). Depending on the light polarization, the electron density evolves differently to reach the excited state. For example, if the electric



field is polarized along the [100] direction, an electron from the As atom can move towards any one of its four nearest neighboring Ga atoms with equal probability, generating no net current. If the polarization is along the [111] direction, an electron from the As atom will move primarily towards its closest neighboring Ga atom in the [111] direction, generating a net current [173].

The shift current requires the breaking of inversion symmetry. But, again, this is not sufficient. Detailed symmetry analysis [164] shows that among the 21 crystal classes that lack inversion symmetry, 20 classes can support the shift current; the only exception is 432. Thus the shift current exists in GaAs and other zinc-blende ($\bar{4}3m$) semiconductors [184]. Different from the injection current, the shift current can be generated with linearly polarized light.

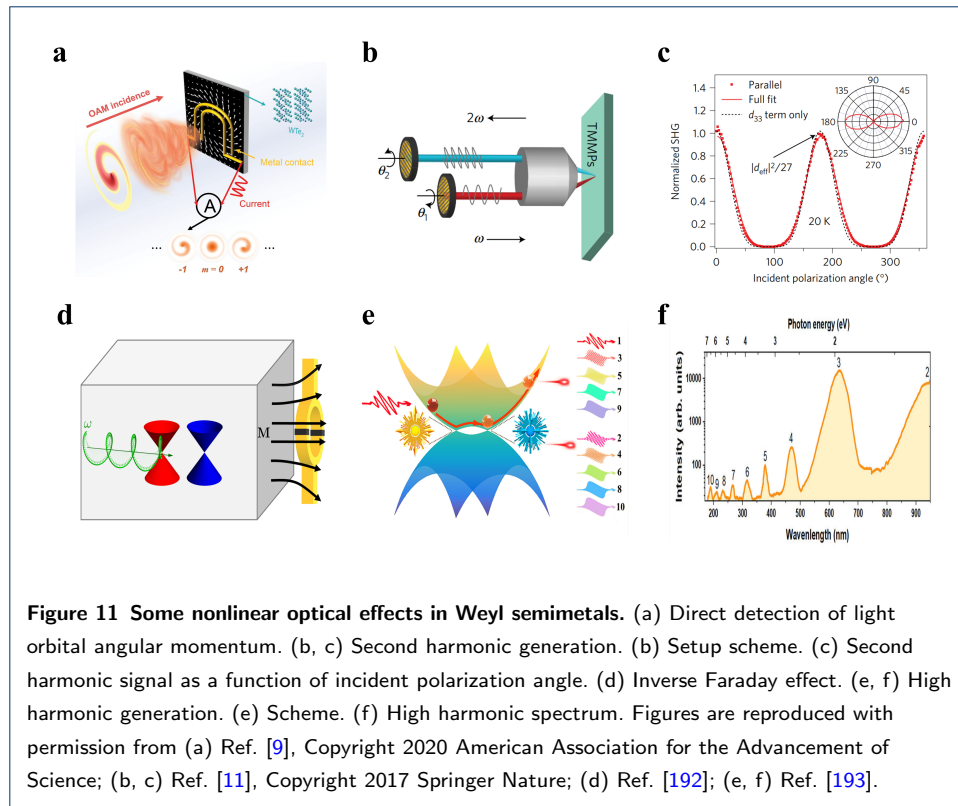
The shift current in Weyl semimetals has been investigated both theoretically [155, 175] and experimentally [168, 185]. In Ref. [168], Osterhoudt et al. report the experimental observation of the shift current in the Weyl semimetal TaAs. Their setup is similar to that in Fig. 9e: a photocurrent microscope equipped with a CO₂ laser, where the light polarization is controlled by the rotation angle ϕ of the quarter-wave plate (Fig. 10c). Their sample is different from the bulk crystal in Fig. 9f: The TaAs sample is fabricated into a microscopic device (Fig. 10d) with a small area (20 times smaller than the laser spot) and a small thickness (only three times the penetration depth ~ 250 nm of the light). This design mitigates the resistive losses and thermal effects. The sample is kept at room temperature, hence the scattering time τ is short, and the shift current dominates over the injection current [see Eq. (42)]. Despite the careful design of the device, the photo-thermal effect cannot be eliminated. Fortunately, one can separate the photo-thermal effect from the shift current by their different polarization dependence. Detailed symmetry analysis shows that for the photocurrent measured along the a axis, the thermal contribution $J_{\text{thermal}}^a = D + L_c \cos 4\phi$ and the shift contribution $J_{\text{shift}}^a = L_s \sin 4\phi$ (Fig. 10e). By fitting the ϕ -dependent photocurrent, one can obtain the parameters D , L_c , and L_s . Fig. 10f shows their measured values as functions of input power, which all exhibit linear dependence. This is as expected since both mechanisms of the shift current and the photo-thermal effect rely on the square of the electric field.

Third, we briefly discuss the anomalous current. The anomalous current arises from the anomalous velocity [186, 187] caused by the Berry curvature [29, 153, 188,

[189]. Similar to the injection current, the anomalous current is generated only with elliptically polarized light, and changes sign when the helicity of light flips [165]. The anomalous current in Weyl semimetals was theoretically predicted but not experimentally observed yet. We refer readers to Ref. [165] for detailed theoretical analysis.

Finally, we point out that the Fermi arc states may induce additional contribution to the photocurrent generation. See Refs. [190, 191] for more details.

3.2.2 Orbital angular momentum detection



Light can carry orbital angular momentum (OAM) [194]. The OAM manifests as a helical wavefront with an azimuthal phase distribution $e^{im\phi}$ where m is the mode number and ϕ is the azimuthal angle. The OAM modes of light can encode information. However, direct detection of OAM by the photocurrent measurement is challenging. This is because most types of photocurrents are sensitive only to optical intensity, not to optical phase.

In Ref. [195], Quintero *et al.* propose a new mechanism for the generation of photocurrent, called the orbital photogalvanic effect. In this case, the incident light can

transfer its OAM and energy simultaneously to the electrons. This process is similar to the photon drag effect [196], where the linear momentum of absorbed photons is transferred to electrons. Because the optical phase varies in the azimuthal direction, it induces a spatial imbalance of excited carriers, producing a net current flowing either along or perpendicular to the helical phase gradient. The generated photocurrent is proportional to the OAM; when the OAM reverses signs, the photocurrent also flips direction.

In Ref. [9], Ji et al. utilize the orbital photogalvanic effect to enable direct on-chip electric readout of OAM. They fabricate electrodes of various shapes on WTe_2 for use as photocurrent detectors (Fig. 11a). WTe_2 is a room-temperature Weyl semimetal with broken inversion symmetry. It is an ideal material for observing the orbital photocurrent because it has large nonlinear optical susceptibilities and certain symmetries that forbid the photocurrents of other types. In the experiment, Ji et al. observe that the photocurrent displays steplike changes with different OAM. Such a detector can be exploited in future photonic circuits for optical communications. In Ref. [10], Lai et al. demonstrate the generation of orbital photocurrents in the mid-infrared wavelengths with another Weyl semimetal TaIrTe_4 .

3.2.3 Second harmonic generation

Second harmonic generation is another important second-order nonlinear optical effect. It refers to the generation of photons with twice the frequency of the incident light. Recent works [11, 197] show that noncentrosymmetric Weyl semimetals can exhibit strong second harmonic generation.

In Ref. [11], Wu et al. reveal giant second harmonic generation in the Weyl semimetals TaAs, TaP, and NbAs. These materials belong to the point group $4mm$, which has a unique polar (z) axis along the [001] direction. Symmetry analysis shows that second harmonic generation is allowed when the incident electric field has a nonzero z -component. Fig. 11b depicts the schematic setup. The incident pulses of 800 nm wavelength are focused at near-normal incidence on the (112) surface of the sample. The generated second-harmonic light is detected in the reflection. The polarization of the incident light and the second-harmonic light are controlled by two sets of polarizers and waveplates, referred to as the generator and the analyzer, respectively. Angles θ_1 and θ_2 denote the angles of the linear polarization plane after

the generator and the analyzer, respectively, with respect to the $[1, 1, -1]$ crystal axis. Fig. 11c shows the normalized second harmonic intensity as a function of θ_1 when $\theta_1 = \theta_2$ at 20 K, while the inset shows the polar plot. The data is consistent with the symmetry analysis and can be fitted well with the theoretical prediction. The second harmonic signal is highly anisotropic and sensitive to the incident polarization: It reaches the maximum at $\theta_1 = 0^\circ$ or 180° when the electric field is along the $[1, 1, -1]$ direction and has the largest z -component; it reaches the minimum at $\theta_1 = 90^\circ$ or 270° when the electric field is along the $[1, -1, 0]$ direction and has zero z -component. The second harmonic signal is giant: The second-order optical susceptibility $\chi^{(2)}$ has the largest component of 7200 pmV^{-1} , which is larger by almost one order of magnitude than the value in the archetypal electro-optic materials GaAs (700 pmV^{-1}) and ZnTe (900 pmV^{-1}), even when measured at wavelengths where their response is the largest. In fact, such a value is larger than then reported in any crystal. In Ref. [197], Patankar et al. further investigate the physical origins of such a giant second harmonic generation in TaAs.

From a practical perspective, Weyl semimetals are not optimal for frequency-doubling applications in the visible regime because of their strong absorption. However, they are promising materials for terahertz generation [198] and optoelectronic devices such as far-infrared detectors because the loss is lower at these longer wavelengths.

3.2.4 Inverse Faraday effect

The inverse Faraday effect is the reverse of the Faraday effect. Recall that the Faraday effect refers to the polarization rotation of light induced by a static magnetization along the light propagation direction [113]. Correspondingly, the inverse Faraday effect refers to the generation of static magnetization induced by circularly polarized light propagating inside the material (Fig. 11d) [199, 200]. In this case, the angular momentum from an oscillating electric field $\mathbf{E}(t)$ is transferred into the magnetic moment of electrons, leading to a static magnetization $\mathbf{M} \propto \mathbf{E}(\omega) \times \mathbf{E}^*(\omega)$. The inverse Faraday effect is a nonlinear phenomenon [201]. It does not require absorption but is rather based on a Raman-like coherent optical scattering process. Consequently, this effect is non-thermal and takes place on a femtosecond timescale. The laser-induced magnetization can be used for ultrafast control of magnetic de-

vices [202, 203]. It can also cause the Faraday rotation for a subsequent *probe* light, which induces a matter-mediated light-light interaction.

Recent works [204, 205, 206, 207, 208] show that Dirac and Weyl semimetals can exhibit a strong inverse Faraday effect due to their unique carrier transport properties and strong spin-orbit coupling. For example, in Ref. [206], Tokman *et al.* estimate that in a Weyl semimetal with n Weyl nodes and a Fermi energy of 100 meV, an incident pump light with an electric field 10 kV/cm at a frequency 1 THz can induce a magnetization that causes the Faraday rotation parameter $\alpha \approx 6.6n^{3/2}$ rad/cm for a probe light. Such a value is two orders of magnitude larger than that obtained in typical ferrites [203].

In Ref. [192], Liang *et al.* propose an unconventional mechanism of inverse Faraday effect in Dirac and Weyl semimetals, referred to as the “axial magnetoelectric effect”. As we discussed above, in the conventional inverse Faraday effect, static magnetization is generated through dynamical electromagnetic fields. In contrast, in the axial magnetoelectric effect, static magnetization is generated through dynamical axial gauge fields. Such effective gauge fields can be generated in a Dirac or Weyl semimetal via dynamical deformations (sound). They interact with electrons similarly to the usual electromagnetic fields but with different signs for different chiralities (see Ref. [4] for an introduction to axial gauge fields). In the axial magnetoelectric effect, the angular momentum is transferred from the axial or pseudoelectric field, conventionally denoted as $\mathbf{E}_5(t)$, into the magnetic moment of electrons, leading to a static magnetization $\mathbf{M} \propto \mathbf{E}_5(\omega) \times \mathbf{E}_5^*(\omega)$. The synthetic nature of the axial gauge fields means that one can induce magnetization in Dirac and Weyl semimetals using phonons without any electromagnetic fields.

3.2.5 Higher-order nonlinear effects

Weyl semimetals can also exhibit higher-order nonlinear optical effects, such as four-wave mixing, optical Kerr effect, and high-harmonic generation. These nonlinear effects are expected to be strong, especially at long wavelengths, due to the linear dispersion and high mobility of the Weyl fermions. Moreover, these effects may exhibit nontrivial features due to the anomalous Berry curvature associated with the Weyl nodes.

In Ref. [12], Almutairi et al. derive the third-order nonlinear optical conductivity of Weyl semimetals in the long-wavelength limit and calculate the intensity of the nonlinear four-wave mixing signal. The calculated nonlinear generation efficiency is surprisingly high for a lossy material, of the order of several mW per W^3 of the incident pump power. This value is many orders of magnitude higher than in conventional nonlinear materials [162]. Optimal conditions for the four-wave mixing are realized in the vicinity of bulk plasma resonance. This work indicates that ultrathin Weyl semimetal films of the order of skin depth in thickness can find applications in compact nonlinear optoelectronic devices.

In Ref. [13], Cheng et al. derive the analytic expressions for linear and third-order optical conductivities of Dirac and Weyl semimetals, and compare the results with those of two-dimensional Dirac materials such as graphene. The details of the third-order conductivity are discussed for third-harmonic generation, the Kerr effect and two-photon carrier injection, parametric frequency conversion, and two-color coherent current injection. In contrast with two-dimensional materials, the three-dimensional Dirac and Weyl semimetals allow for adjusting the nonlinear signals by tuning the sample thickness. Thus, one can envision broad applications of such materials in nonlinear photonic devices.

In Ref. [193], Lv et al. report the experimental observation of high-harmonic generation in Weyl semimetal β -WP₂. High-harmonic generation in solids has only been discovered recently [209, 210, 211, 212]. Recent works [213, 214] report efficient high-harmonic generation from topological materials. Moreover, Ref. [215] shows that the polarimetry of high-harmonic emission from solids can be used to directly retrieve the Berry curvature. In Lv's experiment, both odd and even orders of high-harmonic emissions are observed (Fig. 11f). The high-harmonic spectrum extends into the vacuum ultraviolet region (190 nm, 10th order) even under fairly low femtosecond laser intensity (~ 0.29 TW/cm²). It is interpreted that odd-order harmonics come from the Bloch oscillation, while even-order harmonics arise from the effective Lorentz force due to the Berry curvature (Fig. 11e). By analyzing the crystallographic orientation-dependent high-harmonic spectra, they further quantitatively retrieve the electronic band structure and Berry curvature of β -WP₂.

3.3 Other effects

Of course, this tutorial review cannot cover all the reported optical phenomena and applications of Weyl semimetals. Here we list some examples of other phenomena and applications not covered in this review: gyrotropic magnetic effect [216], photoinduced anomalous Hall effect [217], nonlinear magneto-optical effects [156], topological frequency conversion [218], emergent electromagnetic induction [219, 220], tunable perfect absorption [221], unidirectional bound states in the continuum [222], transverse Kerker effect [223], and topological lasers [224].

4 Thermal photonic applications and devices

In this section, we survey various thermal photonic applications of Weyl semimetals. We discuss the nonreciprocal thermal emitters in Sec. 4.1, the heat flux control in Sec. 4.2, and the control of Casimir force in Sec. 4.3.

4.1 Nonreciprocal thermal emitters

Conventional thermal emitters obey Kirchhoff's law of thermal radiation [104, 225, 226, 227, 228, 229], which states that for a given direction, polarization, and frequency, the emissivity and the absorptivity are equal. However, Kirchhoff's law is not a requirement of thermodynamics but a consequence of Lorentz reciprocity [230, 111, 231, 112]. One can construct thermal emitters with nonreciprocal materials featuring an asymmetric dielectric tensor. A conventional way to achieve the nonreciprocal effect is to use the nonreciprocal response of magneto-optical materials under an external magnetic field. The cyclotron motion of electrons breaks the microscopic reversibility [232, 233], resulting in different properties when the medium is absorbing and emitting light [234, 235]. Using this strategy, Zhu and Fan [236] proposed a photonic thermal emitter that can achieve complete violation of Kirchhoff's law. However, since the nonreciprocal effect is quite weak in the thermal radiation wavelength range ($\sim 10 \mu\text{m}$ at room temperature), the nonreciprocal emitters require a very large external magnetic field of 3 T to operate. Later, Zhao *et al.* [231] improved the photonic design and reduced the required magnetic field to 0.3 T at the expense of reduced bandwidth of the nonreciprocal effect.

As we mentioned in Sec. 2.5, magnetic Weyl semimetals can exhibit much stronger nonreciprocal effects compared to conventional magneto-optical materials. Such giant nonreciprocity persists at the temperature below the Curie temperature (T_C)

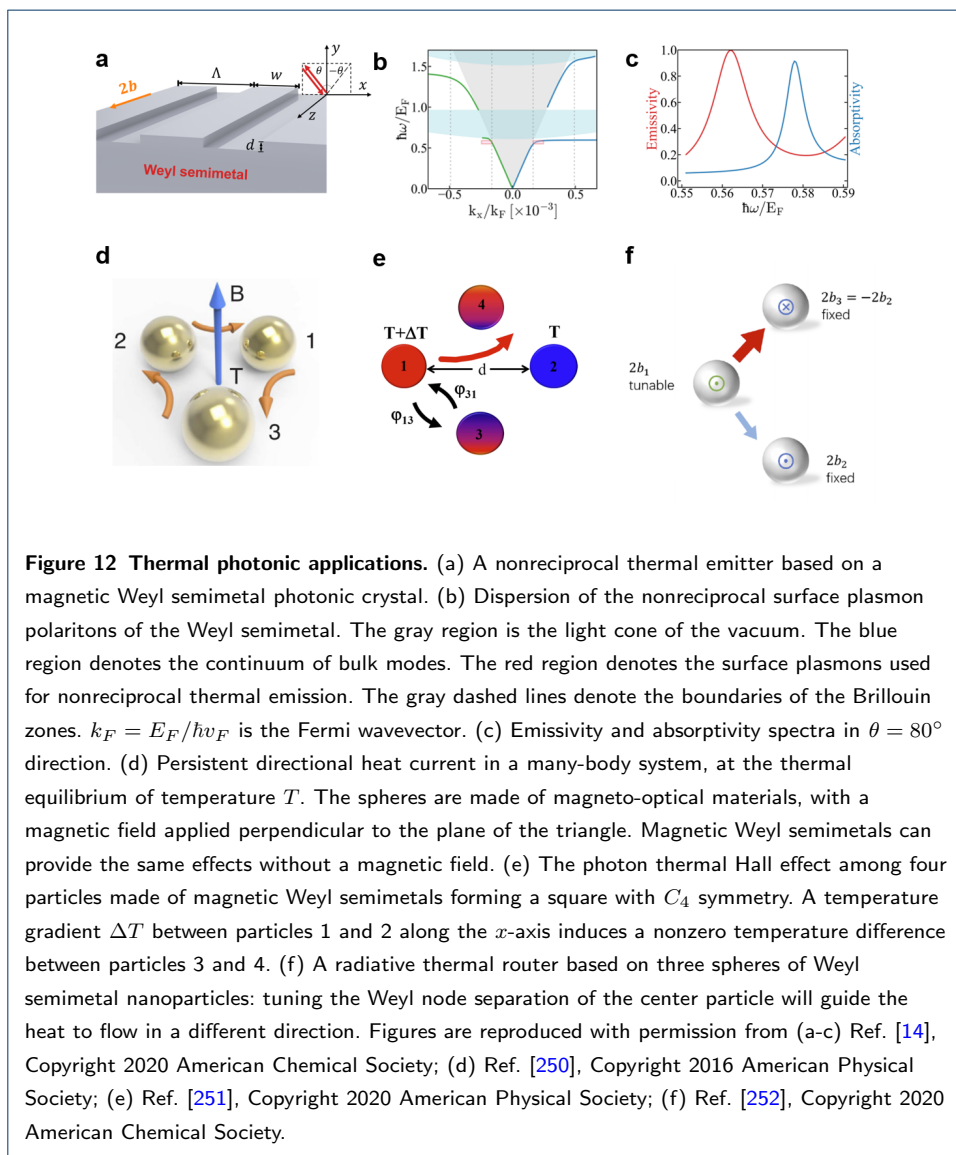
of the material [237]. Some of the known magnetic Weyl semimetals possess high Curie temperature; for example, Co_2MnGa has $T_C = 694\text{ K}$ [237], and Ti_2MnAl has $T_C > 650\text{ K}$ [238, 239]. These materials are ideal candidates for nonreciprocal thermal emission. In Ref. [14], Zhao *et al.* proposed a broadband thermal emitter based on magnetic Weyl semimetals that achieves near-complete violation of Kirchhoff's law at room temperatures. The structure is shown in Fig. 12a which supports nonreciprocal surface plasmon polaritons as shown in Fig. 12b. The emissivity and absorptivity of the emitter show a significant difference as shown in Fig. 12c. Tsurimaki *et al.* investigated the effect of the Fermi-arc surface state and the number of Weyl nodes for Weyl semimetal-based nonreciprocal thermal emitters [15, 16]. Wu *et al.* construct nonreciprocal thermal emitters using Weyl semimetal thin films [240, 241, 242]. Since the nonreciprocal effect is intrinsic to the materials, these thermal emitters do not require any external magnetic field.

Here we note that for a nonreciprocal thermal emitter, the emissivity and absorptivity in the same direction can be different; however, the angular distribution of emissivity and absorptivity can be still constrained by compound symmetries as revealed in Ref. [112]. The compound symmetry can be used to design nonreciprocal thermal emitters with correlated patterns of emissivity and absorptivity [8]. Breaking the compound symmetries can remove such correlation constraints [243, 112].

The above-mentioned works primarily focus on linear polarized thermal radiation. It has been shown that unpatterned thermal emitters with nonreciprocal responses could radiate thermal photons that carry a net spin angular momentum [244, 245, 246]. Khandekar *et al.* studied spin-resolved Kirchhoff's laws in nonreciprocal systems [247]. Since these thermal photons can carry nonzero spin angular momentum, the emission of such photons can result in a back-action torque on the thermal emitter [244, 248]. Maghrebi *et al.* discussed this fluctuation-driven torque for a topological insulator thin film out of thermal equilibrium with a cold environment [244]. Guo and Fan proposed a single-particle heat engine utilizing this effect [249].

4.2 Heat flux control

Radiative heat transfer plays an important role in photon-based energy conversion and thermal management systems [226, 253]. In traditional thermal systems, the



radiative heat flux is driven by a nonzero temperature gradient, and the radiative heat transfer is reciprocal, indicating that when the temperatures of two bodies are exchanged, the magnitude of the heat flux transferred between them is unchanged. However, in systems that involve nonreciprocal materials, photons can flow under zero temperature gradient, and radiative heat transfer could be nonreciprocal.

In Ref. [250], Zhu and Fan reported the existence of a persistent photon heat current in a nonreciprocal multi-body system even without a temperature gradient. As shown in Fig. 12d, the arrows indicate the net heat flux direction when the three magneto-optical spheres are at the same temperature. Later, the persistent heat current feature was also reported within a single nonreciprocal body or cavity [254, 248, 255]. This phenomenon is closely related to the thermal Hall effect [256, 257]. In Ref. [258], Ben-Abdallah reported that with an external magnetic field, nonzero heat flux is induced in the direction that is perpendicular to the temperature gradient between magneto-optical spheres, as illustrated in Fig. 12e. In Ref. [251], Ott *et al.* reported the same phenomenon in a multi-body system made of magnetic Weyl semimetals without the need for an external magnetic field.

Optical nonreciprocity can also enable efficient heat rectification [259], as reported in Refs. [260, 261, 262]. These thermal diodes rely on the nonreciprocal optical surface modes or bulk modes that induce an asymmetric thermal resistance. When the temperature gradient alters direction, the magnitude of the thermal resistance also changes.

Magnetic Weyl semimetals also provide new opportunities for controlling near-field radiative heat transfer due to their anisotropic optical properties and flexible tunability. In Ref. [263], Tang *et al.* reported a twist-induced near-field heat modulator based on magnetic Weyl semimetals. The radiative resistance of the system experiences a significant change depending on the relative alignment of the directions of Weyl nodes separation in the thermal emitter and receiver. Other properties of Weyl semimetals such as the Fermi level, the number of Weyl nodes, the Weyl node separations [264], and external magnetic field [265, 252] can also be used to modulate near-field heat transfer. Using these effects, in Ref. [252], Guo demonstrated a radiative thermal router based on Weyl semimetals as illustrated in Fig. 12f. We also note several recent reports concerning the general properties of these radiative heat transfer systems involving nonreciprocal bodies [266, 267, 256, 257, 268].

4.3 Casimir force control

Besides the exciting opportunities in heat transfer, magnetic Weyl semimetals also provide an effective way to control Casimir forces [269, 270, 271, 272], especially to create repulsive Casimir force, a long sought-after effect [273, 274, 275]. In Ref. [269], Wilson *et al.* reported repulsive Casimir force between semi-infinite magnetic Weyl semimetals when the separation of the two semimetals $d \leq 4c/\sigma_{xy}$, where c is the speed of light in the vacuum, and σ_{xy} is the bulk hall conductivity of Weyl semimetals. Recently, it was shown that the equilibrium Casimir force in nonreciprocal systems can be used for propulsion [276]. We expect that an enhanced propulsion effect can be realized in magnetic Weyl semimetals.

Conclusion

In conclusion, we have provided an introductory review of Weyl semimetals in photonics. We covered the basic concept and optical properties of Weyl semimetals, and surveyed their emerging applications in photonic science and engineering. We discussed how the nontrivial topology of Weyl semimetals leads to unusual optical properties. Photonics based on Weyl semimetals is an emerging topic with many open challenges and new opportunities. We believe that more exciting applications of Weyl semimetals will come up in the near future, and we wish this pedagogical review will benefit upcoming researchers exploring this new direction.

Declarations

Availability of data and materials

Not applicable.

Competing interests

The authors declare that they have no competing interests.

Funding

This work is supported by MURI projects from the U. S. Army Research Office (Grant No. W911NF-19-1-0279) and the U. S. Air Force Office of Scientific Research (FA9550-21-1-0244).

Author's contributions

CG, VSA, BZ, and SF wrote the manuscript. CG led the collaboration. SF supervised the work.

Acknowledgements

Not applicable.

Author details

¹Department of Applied Physics, Stanford University, 94305 Stanford, California, USA. ²Ginzton Laboratory and Department of Electrical Engineering, Stanford University, 94305 Stanford, California, USA. ³Department of Electronics and Nanoengineering, Aalto University, 02150 Espoo, Finland. ⁴Department of Mechanical Engineering, University of Houston, 77204 Houston, Texas, USA.

References

- Herring, C.: Accidental degeneracy in the energy bands of crystals. *Physical Review* **52**, 365–373 (1937). doi:[10.1103/PhysRev.52.365](https://doi.org/10.1103/PhysRev.52.365)
- Armitage, N.P., Mele, E.J., Vishwanath, A.: Weyl and Dirac semimetals in three-dimensional solids. *Reviews of Modern Physics* **90**, 015001 (2018). doi:[10.1103/RevModPhys.90.015001](https://doi.org/10.1103/RevModPhys.90.015001)
- Srednicki, M.: *Quantum Field Theory*. Cambridge University Press, Cambridge (2007)
- Gorbar, E.V., Miranskij, V.A., Shovkovy, I.A., Sukhachov, P.O.: *Electronic Properties of Dirac and Weyl Semimetals*. World Scientific, Singapore (2021)
- Nagaosa, N., Morimoto, T., Tokura, Y.: Transport, magnetic and optical properties of Weyl materials. *Nature Reviews Materials* **5**, 621–636 (2020). doi:[10.1038/s41578-020-0208-y](https://doi.org/10.1038/s41578-020-0208-y)
- Kotov, O.V., Lozovik, Y.E.: Giant tunable nonreciprocity of light in Weyl semimetals. *Physical Review B* **98**(19), 195446 (2018). doi:[10.1103/PhysRevB.98.195446](https://doi.org/10.1103/PhysRevB.98.195446)
- Asadchy, V.S., Guo, C., Zhao, B., Fan, S.: Sub-wavelength passive optical isolators using photonic structures based on Weyl semimetals. *Advanced Optical Materials* **8**, 2000100 (2020). doi:[10.1002/adom.202000100](https://doi.org/10.1002/adom.202000100)
- Park, Y., Asadchy, V.S., Zhao, B., Guo, C., Wang, J., Fan, S.: Violating Kirchhoff's law of thermal radiation in semitransparent structures. *ACS Photonics* **8**, 2417–2424 (2021). doi:[10.1021/acsp Photonics.1c00612](https://doi.org/10.1021/acsp Photonics.1c00612)
- Ji, Z., Liu, W., Krylyuk, S., Fan, X., Zhang, Z., Pan, A., Feng, L., Davydov, A., Agarwal, R.: Photocurrent detection of the orbital angular momentum of light. *Science* **368**(6492), 763–767 (2020). doi:[10.1126/science.aba9192](https://doi.org/10.1126/science.aba9192)
- Lai, J., Ma, J., Fan, Z., Song, X., Yu, P., Liu, Z., Zhang, P., Shi, Y., Cheng, J., Sun, D.: Direct light orbital angular momentum detection in mid-infrared based on the type-II Weyl semimetal TaIrTe₄. *Advanced Materials* **34**(29), 2201229 (2022). doi:[10.1002/adma.202201229](https://doi.org/10.1002/adma.202201229)
- Wu, L., Patankar, S., Morimoto, T., Nair, N.L., Thewalt, E., Little, A., Analytis, J.G., Moore, J.E., Orenstein, J.: Giant anisotropic nonlinear optical response in transition metal monpnictide Weyl semimetals. *Nature Physics* **13**(4), 350–355 (2017). doi:[10.1038/nphys3969](https://doi.org/10.1038/nphys3969)
- Almutairi, S., Chen, Q., Tokman, M., Belyanin, A.: Four-wave mixing in Weyl semimetals. *Physical Review B* **101**(23), 235156 (2020). doi:[10.1103/PhysRevB.101.235156](https://doi.org/10.1103/PhysRevB.101.235156)
- Cheng, J.L., Sipe, J.E., Wu, S.W.: Third-order optical nonlinearity of three-dimensional massless Dirac fermions. *ACS Photonics* **7**, 2515–2526 (2020). doi:[10.1021/acsp Photonics.0c00836](https://doi.org/10.1021/acsp Photonics.0c00836)
- Zhao, B., Guo, C., Garcia, C.A.C., Narang, P., Fan, S.: Axion-field-enabled nonreciprocal thermal radiation in Weyl semimetals. *Nano Letters* **20**, 1923–1927 (2020). doi:[10.1021/acs.nanolett.9b05179](https://doi.org/10.1021/acs.nanolett.9b05179)
- Tsurimaki, Y., Qian, X., Pajovic, S., Han, F., Li, M., Chen, G.: Large nonreciprocal absorption and emission of radiation in type-I Weyl semimetals with time reversal symmetry breaking. *Physical Review B* **101**, 165426 (2020). doi:[10.1103/PhysRevB.101.165426](https://doi.org/10.1103/PhysRevB.101.165426)
- Pajovic, S., Tsurimaki, Y., Qian, X., Chen, G.: Intrinsic nonreciprocal reflection and violation of Kirchhoff's law of radiation in planar type-I magnetic Weyl semimetal surfaces. *Physical Review B* **102**, 165417 (2020). doi:[10.1103/PhysRevB.102.165417](https://doi.org/10.1103/PhysRevB.102.165417)
- Ashcroft, N.W., Mermin, N.D.: *Solid State Physics*. Holt, Rinehart and Winston, New York (1976)
- Burns, G.: *Solid State Physics*. Academic Press, Boston (1990)
- Golin, S.: Band structure of bismuth: Pseudopotential approach. *Physical Review* **166**, 643–651 (1968). doi:[10.1103/PhysRev.166.643](https://doi.org/10.1103/PhysRev.166.643)
- Slonczewski, J.C., Weiss, P.R.: Band structure of graphite. *Physical Review* **109**, 272–279 (1958). doi:[10.1103/PhysRev.109.272](https://doi.org/10.1103/PhysRev.109.272)
- Weyl, H.: Elektron und gravitation. I. *Zeitschrift für Physik* **56**, 330–352 (1929). doi:[10.1007/BF01339504](https://doi.org/10.1007/BF01339504)
- Super-Kamiokande Collaboration: Evidence for oscillation of atmospheric neutrinos. *Physical Review Letters* **81**, 1562–1567 (1998). doi:[10.1103/PhysRevLett.81.1562](https://doi.org/10.1103/PhysRevLett.81.1562)

23. Vishwanath, A.: Where the Weyl Things Are. *Physics* **8**, 84 (2015)
24. Nielsen, H.B., Ninomiya, M.: Absence of neutrinos on a lattice: (I). Proof by homotopy theory. *Nuclear Physics B* **185**, 20–40 (1981). doi:[10.1016/0550-3213\(81\)90361-8](https://doi.org/10.1016/0550-3213(81)90361-8)
25. Nielsen, H.B., Ninomiya, M.: Absence of neutrinos on a lattice: (II). Intuitive topological proof. *Nuclear Physics B* **193**, 173–194 (1981). doi:[10.1016/0550-3213\(81\)90524-1](https://doi.org/10.1016/0550-3213(81)90524-1)
26. Nielsen, H.B., Ninomiya, M.: A no-go theorem for regularizing chiral fermions. *Physics Letters B* **105**, 219–223 (1981). doi:[10.1016/0370-2693\(81\)91026-1](https://doi.org/10.1016/0370-2693(81)91026-1)
27. Sun, X.-Q., Xiao, M., Bzdušek, T., Zhang, S.-C., Fan, S.: Three-Dimensional Chiral Lattice Fermion in Floquet Systems. *Physical Review Letters* **121**, 196401 (2018). doi:[10.1103/PhysRevLett.121.196401](https://doi.org/10.1103/PhysRevLett.121.196401)
28. von Neuman, J., Wigner, E.: Über merkwürdige diskrete Eigenwerte. Über das Verhalten von Eigenwerten bei adiabatischen Prozessen. *Physikalische Zeitschrift* **30**, 467–470 (1929)
29. Vanderbilt, D.: *Berry Phases in Electronic Structure Theory*. Cambridge University Press, Cambridge (2018)
30. Belopolski, I., Xu, S.-Y., Sanchez, D.S., Chang, G., Guo, C., Neupane, M., Zheng, H., Lee, C.-C., Huang, S.-M., Bian, G., Alidoust, N., Chang, T.-R., Wang, B., Zhang, X., Bansil, A., Jeng, H.-T., Lin, H., Jia, S., Hasan, M.Z.: Criteria for directly detecting topological Fermi arcs in Weyl semimetals. *Physical Review Letters* **116**, 066802 (2016). doi:[10.1103/PhysRevLett.116.066802](https://doi.org/10.1103/PhysRevLett.116.066802)
31. Xu, S.-Y., Belopolski, I., Sanchez, D.S., Neupane, M., Chang, G., Yaji, K., Yuan, Z., Zhang, C., Kuroda, K., Bian, G., Guo, C., Lu, H., Chang, T.-R., Alidoust, N., Zheng, H., Lee, C.-C., Huang, S.-M., Hsu, C.-H., Jeng, H.-T., Bansil, A., Neupert, T., Komori, F., Kondo, T., Shin, S., Lin, H., Jia, S., Hasan, M.Z.: Spin polarization and texture of the Fermi arcs in the Weyl fermion semimetal TaAs. *Physical Review Letters* **116**, 096801 (2016). doi:[10.1103/PhysRevLett.116.096801](https://doi.org/10.1103/PhysRevLett.116.096801)
32. Yan, B., Felser, C.: Topological materials: Weyl semimetals. *Annual Review of Condensed Matter Physics* **8**(1), 337–354 (2017). doi:[10.1146/annurev-conmatphys-031016-025458](https://doi.org/10.1146/annurev-conmatphys-031016-025458)
33. Kramers, H.A.: Théorie générale de la rotation paramagnétique dans les cristaux. *Proceedings Koninklijke Akademie van Wetenschappen* **33**, 959–972 (1930)
34. Xu, S.-Y., Belopolski, I., Alidoust, N., Neupane, M., Bian, G., Zhang, C., Sankar, R., Chang, G., Yuan, Z., Lee, C.-C., Huang, S.-M., Zheng, H., Ma, J., Sanchez, D.S., Wang, B., Bansil, A., Chou, F., Shibaev, P.P., Lin, H., Jia, S., Hasan, M.Z.: Discovery of a Weyl fermion semimetal and topological Fermi arcs. *Science* **349**, 613–617 (2015). doi:[10.1126/science.aaa9297](https://doi.org/10.1126/science.aaa9297)
35. Lv, B.Q., Weng, H.M., Fu, B.B., Wang, X.P., Miao, H., Ma, J., Richard, P., Huang, X.C., Zhao, L.X., Chen, G.F., Fang, Z., Dai, X., Qian, T., Ding, H.: Experimental discovery of Weyl semimetal TaAs. *Physical Review X* **5**, 031013 (2015). doi:[10.1103/PhysRevX.5.031013](https://doi.org/10.1103/PhysRevX.5.031013)
36. Xu, S.-Y., Belopolski, I., Sanchez, D.S., Zhang, C., Chang, G., Guo, C., Bian, G., Yuan, Z., Lu, H., Chang, T.-R., Shibaev, P.P., Prokopovych, M.L., Alidoust, N., Zheng, H., Lee, C.-C., Huang, S.-M., Sankar, R., Chou, F., Hsu, C.-H., Jeng, H.-T., Bansil, A., Neupert, T., Strocov, V.N., Lin, H., Jia, S., Hasan, M.Z.: Experimental discovery of a topological Weyl semimetal state in TaP. *Science Advances* **1**, 1501092 (2015). Chap. Research Article. doi:[10.1126/sciadv.1501092](https://doi.org/10.1126/sciadv.1501092)
37. Zhang, C.-L., Xu, S.-Y., Wang, C.M., Lin, Z., Du, Z.Z., Guo, C., Lee, C.-C., Lu, H., Feng, Y., Huang, S.-M., Chang, G., Hsu, C.-H., Liu, H., Lin, H., Li, L., Zhang, C., Zhang, J., Xie, X.-C., Neupert, T., Hasan, M.Z., Lu, H.-Z., Wang, J., Jia, S.: Magnetic-tunnelling-induced Weyl node annihilation in TaP. *Nature Physics* **13**, 979–986 (2017). doi:[10.1038/nphys4183](https://doi.org/10.1038/nphys4183)
38. Xu, S.-Y., Alidoust, N., Belopolski, I., Yuan, Z., Bian, G., Chang, T.-R., Zheng, H., Strocov, V.N., Sanchez, D.S., Chang, G., Zhang, C., Mou, D., Wu, Y., Huang, L., Lee, C.-C., Huang, S.-M., Wang, B., Bansil, A., Jeng, H.-T., Neupert, T., Kaminski, A., Lin, H., Jia, S., Zahid Hasan, M.: Discovery of a Weyl fermion state with Fermi arcs in niobium arsenide. *Nature Physics* **11**, 748–754 (2015). doi:[10.1038/nphys3437](https://doi.org/10.1038/nphys3437)
39. Zheng, H., Xu, S.-Y., Bian, G., Guo, C., Chang, G., Sanchez, D.S., Belopolski, I., Lee, C.-C., Huang, S.-M., Zhang, X., Sankar, R., Alidoust, N., Chang, T.-R., Wu, F., Neupert, T., Chou, F., Jeng, H.-T., Yao, N., Bansil, A., Jia, S., Lin, H., Hasan, M.Z.: Atomic-scale visualization of quantum interference on a Weyl semimetal surface by scanning tunneling microscopy. *ACS Nano* **10**, 1378–1385 (2016). doi:[10.1021/acsnano.5b06807](https://doi.org/10.1021/acsnano.5b06807)
40. Zheng, H., Chang, G., Huang, S.-M., Guo, C., Zhang, X., Zhang, S., Yin, J., Xu, S.-Y., Belopolski, I., Alidoust, N., Sanchez, D.S., Bian, G., Chang, T.-R., Neupert, T., Jeng, H.-T., Jia, S., Lin, H., Hasan, M.Z.:

- Mirror protected Dirac fermions on a Weyl semimetal NbP surface. *Physical Review Letters* **119**, 196403 (2017). doi:[10.1103/PhysRevLett.119.196403](https://doi.org/10.1103/PhysRevLett.119.196403)
41. Gooth, J., Niemann, A.C., Meng, T., Grushin, A.G., Landsteiner, K., Gotsmann, B., Menges, F., Schmidt, M., Shekhar, C., Süß, V., Hühne, R., Rellinghaus, B., Felser, C., Yan, B., Nielsch, K.: Experimental signatures of the mixed axial–gravitational anomaly in the Weyl semimetal NbP. *Nature* **547**, 324–327 (2017). doi:[10.1038/nature23005](https://doi.org/10.1038/nature23005)
 42. Morali, N., Batabyal, R., Nag, P.K., Liu, E., Xu, Q., Sun, Y., Yan, B., Felser, C., Avraham, N., Beidenkopf, H.: Fermi-arc diversity on surface terminations of the magnetic Weyl semimetal $\text{Co}_3\text{Sn}_2\text{S}_2$. *Science* **365**(6459), 1286–1291 (2019). doi:[10.1126/science.aav2334](https://doi.org/10.1126/science.aav2334)
 43. Belopolski, I., Manna, K., Sanchez, D.S., Chang, G., Ernst, B., Yin, J., Zhang, S.S., Cochran, T., Shumiya, N., Zheng, H., Singh, B., Bian, G., Multer, D., Litskevich, M., Zhou, X., Huang, S.-M., Wang, B., Chang, T.-R., Xu, S.-Y., Bansil, A., Felser, C., Lin, H., Hasan, M.Z.: Discovery of topological Weyl fermion lines and drumhead surface states in a room temperature magnet. *Science* **365**(6459), 1278–1281 (2019). doi:[10.1126/science.aav2327](https://doi.org/10.1126/science.aav2327)
 44. Liu, D.F., Liang, A.J., Liu, E.K., Xu, Q.N., Li, Y.W., Chen, C., Pei, D., Shi, W.J., Mo, S.K., Dudin, P., Kim, T., Cacho, C., Li, G., Sun, Y., Yang, L.X., Liu, Z.K., Parkin, S.S.P., Felser, C., Chen, Y.L.: Magnetic Weyl semimetal phase in a Kagomé crystal. *Science* **365**(6459), 1282–1285 (2019). doi:[10.1126/science.aav2873](https://doi.org/10.1126/science.aav2873)
 45. Fisher, D.J.: *Topological Semimetals*. Materials Research Forum LLC, Millersville (2019)
 46. Xiong, J., Kushwaha, S.K., Liang, T., Krizan, J.W., Hirschberger, M., Wang, W., Cava, R.J., Ong, N.P.: Evidence for the chiral anomaly in the Dirac semimetal Na_3Bi . *Science* **350**, 413–416 (2015). doi:[10.1126/science.aac6089](https://doi.org/10.1126/science.aac6089)
 47. Zhang, C.-L., Xu, S.-Y., Belopolski, I., Yuan, Z., Lin, Z., Tong, B., Bian, G., Alidoust, N., Lee, C.-C., Huang, S.-M., Chang, T.-R., Chang, G., Hsu, C.-H., Jeng, H.-T., Neupane, M., Sanchez, D.S., Zheng, H., Wang, J., Lin, H., Zhang, C., Lu, H.-Z., Shen, S.-Q., Neupert, T., Zahid Hasan, M., Jia, S.: Signatures of the Adler–Bell–Jackiw chiral anomaly in a Weyl fermion semimetal. *Nature Communications* **7**, 10735 (2016). doi:[10.1038/ncomms10735](https://doi.org/10.1038/ncomms10735)
 48. Ong, N.P., Liang, S.: Experimental signatures of the chiral anomaly in Dirac–Weyl semimetals. *Nature Reviews Physics* **3**, 394–404 (2021). doi:[10.1038/s42254-021-00310-9](https://doi.org/10.1038/s42254-021-00310-9)
 49. Zhang, C., Guo, C., Lu, H., Zhang, X., Yuan, Z., Lin, Z., Wang, J., Jia, S.: Large magnetoresistance over an extended temperature regime in monophosphides of tantalum and niobium. *Physical Review B* **92**, 041203 (2015). doi:[10.1103/PhysRevB.92.041203](https://doi.org/10.1103/PhysRevB.92.041203)
 50. Westström, A., Ojanen, T.: Designer curved-space geometry for relativistic fermions in Weyl metamaterials. *Physical Review X* **7**, 041026 (2017). doi:[10.1103/PhysRevX.7.041026](https://doi.org/10.1103/PhysRevX.7.041026)
 51. Cortijo, A., Ferreirós, Y., Landsteiner, K., Vozmediano, M.A.H.: Elastic gauge fields in Weyl semimetals. *Physical Review Letters* **115**, 177202 (2015). doi:[10.1103/PhysRevLett.115.177202](https://doi.org/10.1103/PhysRevLett.115.177202)
 52. Pikulin, D.I., Chen, A., Franz, M.: Chiral anomaly from strain-induced gauge fields in Dirac and Weyl semimetals. *Physical Review X* **6**, 041021 (2016). doi:[10.1103/PhysRevX.6.041021](https://doi.org/10.1103/PhysRevX.6.041021)
 53. Song, Z., Dai, X.: Hear the sound of Weyl fermions. *Physical Review X* **9**, 021053 (2019). doi:[10.1103/PhysRevX.9.021053](https://doi.org/10.1103/PhysRevX.9.021053)
 54. Vafeek, O., Vishwanath, A.: Dirac fermions in solids: From high- T_c cuprates and graphene to topological insulators and Weyl semimetals. *Annual Review of Condensed Matter Physics* **5**, 83–112 (2014). doi:[10.1146/annurev-conmatphys-031113-133841](https://doi.org/10.1146/annurev-conmatphys-031113-133841)
 55. Burkov, A.A.: Weyl metals. *Annual Review of Condensed Matter Physics* **9**, 359–378 (2018). doi:[10.1146/annurev-conmatphys-033117-054129](https://doi.org/10.1146/annurev-conmatphys-033117-054129)
 56. Witzak-Krempa, W., Chen, G., Kim, Y.B., Balents, L.: Correlated quantum phenomena in the strong spin-orbit regime. *Annual Review of Condensed Matter Physics* **5**, 57–82 (2014). doi:[10.1146/annurev-conmatphys-020911-125138](https://doi.org/10.1146/annurev-conmatphys-020911-125138)
 57. Šmejkal, L., Jungwirth, T., Sinova, J.: Route towards Dirac and Weyl antiferromagnetic spintronics. *physica status solidi (RRL) – Rapid Research Letters* **11**, 1700044 (2017). doi:[10.1002/pssr.201700044](https://doi.org/10.1002/pssr.201700044)
 58. Mikitik, G.P., Sharlai, Y.V.: Magnetic susceptibility of topological semimetals. *Journal of Low Temperature Physics* **197**, 272–309 (2019). doi:[10.1007/s10909-019-02225-3](https://doi.org/10.1007/s10909-019-02225-3)

59. Hosur, P., Qi, X.: Recent developments in transport phenomena in Weyl semimetals. *Comptes Rendus Physique* **14**, 857–870 (2013). doi:[10.1016/j.crhy.2013.10.010](https://doi.org/10.1016/j.crhy.2013.10.010)
60. Burkov, A.A.: Chiral anomaly and transport in Weyl metals. *Journal of Physics: Condensed Matter* **27**, 113201 (2015). doi:[10.1088/0953-8984/27/11/113201](https://doi.org/10.1088/0953-8984/27/11/113201)
61. Wang, S., Lin, B.-C., Wang, A.-Q., Yu, D.-P., Liao, Z.-M.: Quantum transport in Dirac and Weyl semimetals: A review. *Advances in Physics: X* **2**, 518–544 (2017). doi:[10.1080/23746149.2017.1327329](https://doi.org/10.1080/23746149.2017.1327329)
62. Gorbar, E.V., Miransky, V.A., Shovkovy, I.A., Sukhachov, P.O.: Anomalous transport properties of Dirac and Weyl semimetals (Review Article). *Low Temperature Physics* **44**, 487–505 (2018). doi:[10.1063/1.5037551](https://doi.org/10.1063/1.5037551)
63. Wang, H., Wang, J.: Electron transport in Dirac and Weyl semimetals. *Chinese Physics B* **27**, 107402 (2018). doi:[2020030514010695](https://doi.org/2020030514010695)
64. Hu, J., Xu, S.-Y., Ni, N., Mao, Z.: Transport of topological semimetals. *Annual Review of Materials Research* **49**, 207–252 (2019). doi:[10.1146/annurev-matsci-070218-010023](https://doi.org/10.1146/annurev-matsci-070218-010023)
65. Chiu, C.-K., Teo, J.C.Y., Schnyder, A.P., Ryu, S.: Classification of topological quantum matter with symmetries. *Reviews of Modern Physics* **88**, 035005 (2016). doi:[10.1103/RevModPhys.88.035005](https://doi.org/10.1103/RevModPhys.88.035005)
66. Witten, E.: Three lectures on topological phases of matter. *La Rivista del Nuovo Cimento* **39**, 313–370 (2016). doi:[10.1393/ncr/i2016-10125-3](https://doi.org/10.1393/ncr/i2016-10125-3)
67. Weng, H., Dai, X., Fang, Z.: Topological semimetals predicted from first-principles calculations. *Journal of Physics: Condensed Matter* **28**, 303001 (2016). doi:[10.1088/0953-8984/28/30/303001](https://doi.org/10.1088/0953-8984/28/30/303001)
68. Hasan, M.Z., Xu, S.-Y., Bian, G.: Topological insulators, topological superconductors and Weyl fermion semimetals: Discoveries, perspectives and outlooks. *Physica Scripta* **T164**, 014001 (2015). doi:[10.1088/0031-8949/2015/T164/014001](https://doi.org/10.1088/0031-8949/2015/T164/014001)
69. Hasan, M.Z., Xu, S.-Y., Belopolski, I., Huang, S.-M.: Discovery of Weyl fermion semimetals and topological Fermi arc states. *Annual Review of Condensed Matter Physics* **8**, 289–309 (2017). doi:[10.1146/annurev-conmatphys-031016-025225](https://doi.org/10.1146/annurev-conmatphys-031016-025225)
70. Yan, B., Felser, C.: Topological materials: Weyl semimetals. *Annual Review of Condensed Matter Physics* **8**, 337–354 (2017). doi:[10.1146/annurev-conmatphys-031016-025458](https://doi.org/10.1146/annurev-conmatphys-031016-025458)
71. Zheng, H., Zahid Hasan, M.: Quasiparticle interference on type-I and type-II Weyl semimetal surfaces: A review. *Advances in Physics: X* **3**, 1466661 (2018). doi:[10.1080/23746149.2018.1466661](https://doi.org/10.1080/23746149.2018.1466661)
72. Nagaosa, N., Sinova, J., Onoda, S., MacDonald, A.H., Ong, N.P.: Anomalous Hall effect. *Reviews of Modern Physics* **82**, 1539–1592 (2010). doi:[10.1103/RevModPhys.82.1539](https://doi.org/10.1103/RevModPhys.82.1539)
73. Gorbar, E.V., Miransky, V.A., Shovkovy, I.A.: Chiral asymmetry of the Fermi surface in dense relativistic matter in a magnetic field. *Physical Review C*, **4** (2009). doi:[10.1103/PhysRevC.80.032801](https://doi.org/10.1103/PhysRevC.80.032801)
74. Zyuzin, A.A., Burkov, A.A.: Topological response in Weyl semimetals and the chiral anomaly. *Physical Review B* **86**(11), 115133 (2012). doi:[10.1103/PhysRevB.86.115133](https://doi.org/10.1103/PhysRevB.86.115133)
75. Nie, S., Hashimoto, T., Prinz, F.B.: Magnetic Weyl semimetal in $K_2Mn_3(AsO_4)_3$ with the minimum number of Weyl points. *Physical Review Letters* **128**, 176401 (2022). doi:[10.1103/PhysRevLett.128.176401](https://doi.org/10.1103/PhysRevLett.128.176401)
76. Soh, J.-R., de Juan, F., Vergniory, M.G., Schröter, N.B.M., Rahn, M.C., Yan, D.Y., Jiang, J., Bristow, M., Reiss, P.A., Blandy, J.N., Guo, Y.F., Shi, Y.G., Kim, T.K., McCollam, A., Simon, S.H., Chen, Y., Coldea, A.I., Boothroyd, A.T.: Ideal Weyl semimetal induced by magnetic exchange. *Physical Review B* **100**, 201102 (2019). doi:[10.1103/PhysRevB.100.201102](https://doi.org/10.1103/PhysRevB.100.201102)
77. Zangwill, A.: *Modern Electrodynamics*. Cambridge University Press, Cambridge (2013)
78. Wilczek, F.: Two applications of axion electrodynamics. *Physical Review Letters* **58**, 1799–1802 (1987). doi:[10.1103/PhysRevLett.58.1799](https://doi.org/10.1103/PhysRevLett.58.1799)
79. Cheng, T.-P., Li, L.-F.: *Gauge Theory of Elementary Particle Physics*. Oxford University Press, Oxford (1984)
80. Volovik, G.E.: *The Universe in a Helium Droplet*. Oxford University Press, Oxford (2009)
81. Qi, X.-L., Hughes, T.L., Zhang, S.-C.: Topological field theory of time-reversal invariant insulators. *Physical Review B* **78**, 195424 (2008). doi:[10.1103/PhysRevB.78.195424](https://doi.org/10.1103/PhysRevB.78.195424)
82. Qi, X.-L., Zhang, S.-C.: Topological insulators and superconductors. *Reviews of Modern Physics* **83**, 1057–1110 (2011). doi:[10.1103/RevModPhys.83.1057](https://doi.org/10.1103/RevModPhys.83.1057)
83. Bernevig, B.A., Hughes, T.L.: *Topological Insulators and Topological Superconductors*. Princeton University Press, Princeton (2013)

84. Grushin, A.G.: Consequences of a condensed matter realization of Lorentz-violating QED in Weyl semi-metals. *Physical Review D* **86**, 045001 (2012). doi:[10.1103/PhysRevD.86.045001](https://doi.org/10.1103/PhysRevD.86.045001)
85. Goswami, P., Tewari, S.: Axionic field theory of (3+1)-dimensional Weyl semimetals. *Physical Review B* **88**, 245107 (2013). doi:[10.1103/PhysRevB.88.245107](https://doi.org/10.1103/PhysRevB.88.245107)
86. Vazifeh, M.M., Franz, M.: Electromagnetic response of Weyl semimetals. *Physical Review Letters* **111**, 027201 (2013). doi:[10.1103/PhysRevLett.111.027201](https://doi.org/10.1103/PhysRevLett.111.027201)
87. Deng, K., Van Dyke, J.S., Minic, D., Heremans, J.J., Barnes, E.: Exploring self-consistency of the equations of axion electrodynamics in Weyl semimetals. *Physical Review B* **104**, 075202 (2021). doi:[10.1103/PhysRevB.104.075202](https://doi.org/10.1103/PhysRevB.104.075202)
88. Armitage, N.P., Wu, L.: On the matter of topological insulators as magnetoelectrics. *SciPost Physics* **6**, 046 (2019). doi:[10.21468/SciPostPhys.6.4.046](https://doi.org/10.21468/SciPostPhys.6.4.046)
89. Tong, D.: Gauge theory. Lecture notes, DAMTP Cambridge (2018)
90. Karch, A.: Electric-magnetic duality and topological insulators. *Physical Review Letters* **103**, 171601 (2009). doi:[10.1103/PhysRevLett.103.171601](https://doi.org/10.1103/PhysRevLett.103.171601)
91. Hofmann, J., Das Sarma, S.: Surface plasmon polaritons in topological Weyl semimetals. *Physical Review B* **93**(24), 241402 (2016). doi:[10.1103/PhysRevB.93.241402](https://doi.org/10.1103/PhysRevB.93.241402)
92. Witten, E.: Fermion path integrals and topological phases. *Reviews of Modern Physics* **88**, 035001 (2016). doi:[10.1103/RevModPhys.88.035001](https://doi.org/10.1103/RevModPhys.88.035001)
93. Fujikawa, K., Suzuki, H.: Path Integrals and Quantum Anomalies. Clarendon Press, Oxford (2013)
94. Kubo, R.: Statistical-mechanical theory of irreversible processes. I. General theory and simple applications to magnetic and conduction problems. *Journal of the Physical Society of Japan* **12**, 570–586 (1957). doi:[10.1143/JPSJ.12.570](https://doi.org/10.1143/JPSJ.12.570)
95. Greenwood, D.A.: The Boltzmann equation in the theory of electrical conduction in metals. *Proceedings of the Physical Society* **71**, 585–596 (1958). doi:[10.1088/0370-1328/71/4/306](https://doi.org/10.1088/0370-1328/71/4/306)
96. Moseley, L.L., Lukes, T.: A simplified derivation of the Kubo-Greenwood formula. *American Journal of Physics* **46**, 676–677 (1978). doi:[10.1119/1.11229](https://doi.org/10.1119/1.11229)
97. Lorentz, H.A.: The theorem of Poynting concerning the energy in the electromagnetic field and two general propositions concerning the propagation of light. *Amsterdamer Akademie der Wetenschappen* **4**, 176 (1896)
98. Potton, R.J.: Reciprocity in optics. *Reports on Progress in Physics* **67**(5), 717–754 (2004). doi:[10.1088/0034-4885/67/5/R03](https://doi.org/10.1088/0034-4885/67/5/R03)
99. Caloz, C., Alù, A., Tretyakov, S., Sounas, D., Achouri, K., Deck-Léger, Z.-L.: Electromagnetic nonreciprocity. *Physical Review Applied* **10**(4), 047001 (2018). doi:[10.1103/PhysRevApplied.10.047001](https://doi.org/10.1103/PhysRevApplied.10.047001)
100. Asadchy, V.S., Mirmoosa, M.S., Díaz-Rubio, A., Fan, S., Tretyakov, S.A.: Tutorial on electromagnetic nonreciprocity and its origins. *Proceedings of the IEEE* **108**, 1684–1727 (2020). doi:[10.1109/JPROC.2020.3012381](https://doi.org/10.1109/JPROC.2020.3012381)
101. Guo, C., Zhao, Z., Fan, S.: Internal transformations and internal symmetries in linear photonic systems. *Physical Review A* **105**, 023509 (2022). doi:[10.1103/PhysRevA.105.023509](https://doi.org/10.1103/PhysRevA.105.023509)
102. Haus, H.A.: *Waves and Fields in Optoelectronics*. Prentice-Hall, Englewood Cliffs, New Jersey (1984)
103. Guo, C., Fan, S.: Reciprocity constraints on reflection. *Physical Review Letters* **128**, 256101 (2022). doi:[10.1103/PhysRevLett.128.256101](https://doi.org/10.1103/PhysRevLett.128.256101)
104. Kirchhoff, G.: Ueber das Verhältniss zwischen dem Emissionsvermögen und dem Absorptionsvermögen der Körper für Wärme und Licht. *Annalen der Physik* **185**(2), 275–301 (1860). doi:[10.1002/andp.18601850205](https://doi.org/10.1002/andp.18601850205)
105. Greffet, J.-J., Bouchon, P., Brucoli, G., Marquier, F.: Light emission by nonequilibrium bodies: Local Kirchhoff law. *Physical Review X* **8**, 021008 (2018). doi:[10.1103/PhysRevX.8.021008](https://doi.org/10.1103/PhysRevX.8.021008)
106. Yu, Z., Fan, S.: Complete optical isolation created by indirect interband photonic transitions. *Nature Photonics* **3**(2), 91–94 (2009). doi:[10.1038/nphoton.2008.273](https://doi.org/10.1038/nphoton.2008.273)
107. Jalas, D., Petrov, A., Eich, M., Freude, W., Fan, S., Yu, Z., Baets, R., Popović, M., Melloni, A., Joannopoulos, J.D., Vanwolleghem, M., Doerr, C.R., Renner, H.: What is – and what is not – an optical isolator. *Nature Photonics* **7**, 579–582 (2013). doi:[10.1038/nphoton.2013.185](https://doi.org/10.1038/nphoton.2013.185)
108. Wang, Z., Fan, S.: Optical circulators in two-dimensional magneto-optical photonic crystals. *Optics Letters* **30**, 1989–1991 (2005). doi:[10.1364/OL.30.001989](https://doi.org/10.1364/OL.30.001989)

109. Wang, Z., Chong, Y., Joannopoulos, J.D., Soljačić, M.: Observation of unidirectional backscattering-immune topological electromagnetic states. *Nature* **461**, 772–775 (2009). doi:[10.1038/nature08293](https://doi.org/10.1038/nature08293)
110. Fang, K., Yu, Z., Fan, S.: Realizing effective magnetic field for photons by controlling the phase of dynamic modulation. *Nature Photonics* **6**(11), 782–787 (2012). doi:[10.1038/nphoton.2012.236](https://doi.org/10.1038/nphoton.2012.236)
111. Zhu, L., Fan, S.: Near-complete violation of detailed balance in thermal radiation. *Physical Review B* **90**(22), 220301 (2014). doi:[10.1103/PhysRevB.90.220301](https://doi.org/10.1103/PhysRevB.90.220301)
112. Guo, C., Zhao, B., Fan, S.: Adjoint Kirchhoff's law and general symmetry implications for all thermal emitters. *Physical Review X* **12**, 021023 (2022). doi:[10.1103/PhysRevX.12.021023](https://doi.org/10.1103/PhysRevX.12.021023)
113. Zvezdin, A.K., Kotov, V.A.: *Modern Magneto-optics and Magneto-optical Materials*. CRC Press, New York (1997)
114. Han, X., Markou, A., Stensberg, J., Sun, Y., Felser, C., Wu, L.: Giant intrinsic anomalous terahertz Faraday rotation in the magnetic Weyl semimetal Co₂MnGa at room temperature. *Physical Review B* **105**, 174406 (2022). doi:[10.1103/PhysRevB.105.174406](https://doi.org/10.1103/PhysRevB.105.174406)
115. Huang, H., Fan, Y., Wu, B.-I., Kong, a.J.: Tunable TE/TM Wave Splitter Using a Gyrotropic Slab. *Progress In Electromagnetics Research* **85**, 367–380 (2008). doi:[10.2528/PIER08080303](https://doi.org/10.2528/PIER08080303)
116. Abdol, S.O., Abdollahipour, B., Vala, A.S.: Surface plasmon polaritons in a waveguide composed of Weyl semimetals with different symmetries. *Journal of Physics D: Applied Physics* **53**(4), 045105 (2019). doi:[10.1088/1361-6463/ab52ee](https://doi.org/10.1088/1361-6463/ab52ee)
117. Ashby, P.E.C., Carbotte, J.P.: Chiral anomaly and optical absorption in Weyl semimetals. *Physical Review B* **89**, 245121 (2014). doi:[10.1103/PhysRevB.89.245121](https://doi.org/10.1103/PhysRevB.89.245121)
118. Huang, J., Wang, L., Yao, D.-X.: A semiclassical approach to surface Fermi arcs in Weyl semimetals. *Science China Physics, Mechanics & Astronomy* **65**, 266811 (2022). doi:[10.1007/s11433-021-1884-x](https://doi.org/10.1007/s11433-021-1884-x)
119. Chen, Q., Kutayiah, A.R., Oladyshkin, I., Tokman, M., Belyanin, A.: Optical properties and electromagnetic modes of Weyl semimetals. *Physical Review B* **99**(7), 075137 (2019). doi:[10.1103/PhysRevB.99.075137](https://doi.org/10.1103/PhysRevB.99.075137)
120. Song, J.C.W., Rudner, M.S.: Fermi arc plasmons in Weyl semimetals. *Physical Review B* **96**, 205443 (2017). doi:[10.1103/PhysRevB.96.205443](https://doi.org/10.1103/PhysRevB.96.205443)
121. Lošić, Ž.B.: The coupling effects of surface plasmons and Fermi arc plasmons in Weyl semimetals. *Journal of Physics: Condensed Matter* **31**, 285001 (2019). doi:[10.1088/1361-648X/ab1734](https://doi.org/10.1088/1361-648X/ab1734)
122. Gomez-Díaz, J.S., Tymchenko, M., Alù, A.: Hyperbolic plasmons and topological transitions over uniaxial metasurfaces. *Physical Review Letters* **114**, 233901 (2015). doi:[10.1103/PhysRevLett.114.233901](https://doi.org/10.1103/PhysRevLett.114.233901)
123. Zhang, F., Gao, Y., Zhang, W.: Three-dimensional topological plasmons in Weyl semimetals. *Physical Review B* **104**, 205141 (2021). doi:[10.1103/PhysRevB.104.205141](https://doi.org/10.1103/PhysRevB.104.205141)
124. Kurokawa, K.: *An Introduction to the Theory of Microwave Circuits*. Academic, New York (1969)
125. Dötsch, H., Bahlmann, N., Zhuromsky, O., Hammer, M., Wilkens, L., Gerhardt, R., Hertel, P., Popkov, A.F.: Applications of magneto-optical waveguides in integrated optics: Review. *Journal of the Optical Society of America B* **22**, 240–253 (2005). doi:[10.1364/JOSAB.22.000240](https://doi.org/10.1364/JOSAB.22.000240)
126. Shoji, Y., Mizumoto, T.: Magneto-optical non-reciprocal devices in silicon photonics. *Science and Technology of Advanced Materials* **15**, 014602 (2014). doi:[10.1088/1468-6996/15/1/014602](https://doi.org/10.1088/1468-6996/15/1/014602)
127. Kravtsov, N.V., Kravtsov, N.N.: Nonreciprocal effects in ring lasers. *Quantum Electronics* **29**, 378 (1999). doi:[10.1070/QE1999v029n05ABEH001495](https://doi.org/10.1070/QE1999v029n05ABEH001495)
128. Liu, E., Sun, Y., Kumar, N., Muechler, L., Sun, A., Jiao, L., Yang, S.-Y., Liu, D., Liang, A., Xu, Q., Kroder, J., Süß, V., Borrmann, H., Shekhar, C., Wang, Z., Xi, C., Wang, W., Schnelle, W., Wirth, S., Chen, Y., Goennenwein, S.T.B., Felser, C.: Giant anomalous Hall effect in a ferromagnetic kagome-lattice semimetal. *Nature Physics* **14**, 1125–1131 (2018). doi:[10.1038/s41567-018-0234-5](https://doi.org/10.1038/s41567-018-0234-5)
129. Figotin, A., Vitebsky, I.: Nonreciprocal magnetic photonic crystals. *Physical Review E* **63**(6), 066609 (2001). doi:[10.1103/PhysRevE.63.066609](https://doi.org/10.1103/PhysRevE.63.066609)
130. Li, T., Yin, C., Wu, F.: Strong optical non-reciprocity in one-dimensional photonic crystal containing a Weyl semimetal-based defect. *Optical Materials* **121**, 111583 (2021). doi:[10.1016/j.optmat.2021.111583](https://doi.org/10.1016/j.optmat.2021.111583)
131. Fan, S., Joannopoulos, J.D.: Analysis of guided resonances in photonic crystal slabs. *Physical Review B* **65**, 235112 (2002). doi:[10.1103/PhysRevB.65.235112](https://doi.org/10.1103/PhysRevB.65.235112)
132. Kargarian, M., Randeria, M., Trivedi, N.: Theory of Kerr and Faraday rotations and linear dichroism in

- topological Weyl semimetals. *Scientific Reports* **5**, 12683 (2015). doi:[10.1038/srep12683](https://doi.org/10.1038/srep12683)
133. Chtchelkatchev, N.M., Berman, O.L., Kezerashvili, R.Y., Lozovik, Y.E.: Chiral filtration of light by Weyl-semimetal medium. *Physics Letters A* **399**, 127294 (2021). doi:[10.1016/j.physleta.2021.127294](https://doi.org/10.1016/j.physleta.2021.127294)
 134. Yang, C., Zhao, B., Cai, W., Zhang, Z.M.: Mid-infrared broadband circular polarizer based on Weyl semimetals. *Optics Express* **30**(2), 3035–3046 (2022). doi:[10.1364/OE.445803](https://doi.org/10.1364/OE.445803)
 135. Mukherjee, S.P., Carbotte, J.P.: Absorption of circular polarized light in tilted type-I and type-II Weyl semimetals. *Physical Review B* **96**, 085114 (2017). doi:[10.1103/PhysRevB.96.085114](https://doi.org/10.1103/PhysRevB.96.085114)
 136. Ukhtary, M.S., Nugraha, A.R.T., Saito, R.: Negative refraction in Weyl semimetals. *Journal of the Physical Society of Japan* **86**(10), 104703 (2017). doi:[10.7566/JPSJ.86.104703](https://doi.org/10.7566/JPSJ.86.104703)
 137. Hills, R.D.Y., Kusmartseva, A., Kusmartsev, F.V.: Current-voltage characteristics of Weyl semimetal semiconducting devices, Veselago lenses, and hyperbolic Dirac phase. *Physical Review B* **95**, 214103 (2017). doi:[10.1103/PhysRevB.95.214103](https://doi.org/10.1103/PhysRevB.95.214103)
 138. Veselago, V.G.: The electrodynamics of substances with simultaneously negative values of ϵ and μ . *Soviet Physics Uspekhi* **10**(4), 509 (1968). doi:[10.1070/PU1968v010n04ABEH003699](https://doi.org/10.1070/PU1968v010n04ABEH003699)
 139. Pendry, J.B.: Negative refraction makes a perfect lens. *Physical Review Letters* **85**(18), 3966–3969 (2000). doi:[10.1103/PhysRevLett.85.3966](https://doi.org/10.1103/PhysRevLett.85.3966)
 140. Shelby, R.A., Smith, D.R., Schultz, S.: Experimental verification of a negative index of refraction. *Science* **292**(5514), 77–79 (2001). doi:[10.1126/science.1058847](https://doi.org/10.1126/science.1058847)
 141. Notomi, M.: Theory of light propagation in strongly modulated photonic crystals: Refractionlike behavior in the vicinity of the photonic band gap. *Physical Review B* **62**, 10696–10705 (2000). doi:[10.1103/PhysRevB.62.10696](https://doi.org/10.1103/PhysRevB.62.10696)
 142. Luo, C., Johnson, S.G., Joannopoulos, J.D., Pendry, J.B.: All-angle negative refraction without negative effective index. *Physical Review B* **65**, 201104 (2002). doi:[10.1103/PhysRevB.65.201104](https://doi.org/10.1103/PhysRevB.65.201104)
 143. Cubukcu, E., Aydin, K., Ozbay, E., Foteinopoulou, S., Soukoulis, C.M.: Negative refraction by photonic crystals. *Nature* **423**, 604–605 (2003). doi:[10.1038/423604b](https://doi.org/10.1038/423604b)
 144. Tretyakov, S., Nefedov, I., Sihvola, A., Maslovski, S., Simovski, C.: Waves and energy in chiral nihility. *Journal of Electromagnetic Waves and Applications* **17**(5), 695–706 (2003). doi:[10.1163/15693930322226356](https://doi.org/10.1163/15693930322226356)
 145. Pendry, J.B.: A chiral route to negative refraction. *Science* **306**, 1353–1355 (2004). doi:[10.1126/science.1104467](https://doi.org/10.1126/science.1104467)
 146. Monzon, C., Forester, D.W.: Negative refraction and focusing of circularly polarized waves in optically active media. *Physical Review Letters* **95**, 123904 (2005). doi:[10.1103/PhysRevLett.95.123904](https://doi.org/10.1103/PhysRevLett.95.123904)
 147. Zhang, S., Park, Y.-S., Li, J., Lu, X., Zhang, W., Zhang, X.: Negative refractive index in chiral metamaterials. *Physical Review Letters* **102**, 023901 (2009). doi:[10.1103/PhysRevLett.102.023901](https://doi.org/10.1103/PhysRevLett.102.023901)
 148. Hayata, T.: A new route to negative refractive index from topological metals. *Progress of Theoretical and Experimental Physics* **2018**, 083–01 (2018). doi:[10.1093/ptep/pty082](https://doi.org/10.1093/ptep/pty082)
 149. Tchoumakov, S., Cayssol, J., Grushin, A.G.: Three-dimensional chiral Veselago lensing. *Physical Review B* **105**(7), 075309 (2022). doi:[10.1103/PhysRevB.105.075309](https://doi.org/10.1103/PhysRevB.105.075309)
 150. Giuliani, G., Vignale, G.: *Quantum Theory of the Electron Liquid*. Cambridge University Press, Cambridge (2005)
 151. Moore, J.E.: Optical properties of Weyl semimetals. *National Science Review* **6**, 206–208 (2019). doi:[10.1093/nsr/nwy164](https://doi.org/10.1093/nsr/nwy164)
 152. Peterson, R.L.: Formal theory of nonlinear response. *Reviews of Modern Physics* **39**, 69–77 (1967). doi:[10.1103/RevModPhys.39.69](https://doi.org/10.1103/RevModPhys.39.69)
 153. Sodemann, I., Fu, L.: Quantum nonlinear Hall effect induced by Berry curvature dipole in time-reversal invariant materials. *Physical Review Letters* **115**, 216806 (2015). doi:[10.1103/PhysRevLett.115.216806](https://doi.org/10.1103/PhysRevLett.115.216806)
 154. Cortijo, A.: Magnetic-field-induced nonlinear optical responses in inversion symmetric Dirac semimetals. *Physical Review B* **94**, 235123 (2016). doi:[10.1103/PhysRevB.94.235123](https://doi.org/10.1103/PhysRevB.94.235123)
 155. Morimoto, T., Nagaosa, N.: Topological nature of nonlinear optical effects in solids. *Science Advances* **2**, 1501524 (2016). doi:[10.1126/sciadv.1501524](https://doi.org/10.1126/sciadv.1501524)
 156. Morimoto, T., Zhong, S., Orenstein, J., Moore, J.E.: Semiclassical theory of nonlinear magneto-optical responses with applications to topological Dirac/Weyl semimetals. *Physical Review B* **94**(24), 245121 (2016).

- doi:[10.1103/PhysRevB.94.245121](https://doi.org/10.1103/PhysRevB.94.245121)
157. Ma, Q., Xu, S.-Y., Chan, C.-K., Zhang, C.-L., Chang, G., Lin, Y., Xie, W., Palacios, T., Lin, H., Jia, S., Lee, P.A., Jarillo-Herrero, P., Gedik, N.: Direct optical detection of Weyl fermion chirality in a topological semimetal. *Nature Physics* **13**, 842–847 (2017). doi:[10.1038/nphys4146](https://doi.org/10.1038/nphys4146)
 158. de Juan, F., Grushin, A.G., Morimoto, T., Moore, J.E.: Quantized circular photogalvanic effect in Weyl semimetals. *Nature Communications* **8**, 15995 (2017). doi:[10.1038/ncomms15995](https://doi.org/10.1038/ncomms15995)
 159. Chan, C.-K., Lindner, N.H., Refael, G., Lee, P.A.: Photocurrents in Weyl semimetals. *Physical Review B* **95**, 041104 (2017). doi:[10.1103/PhysRevB.95.041104](https://doi.org/10.1103/PhysRevB.95.041104)
 160. König, E.J., Xie, H.-Y., Pesin, D.A., Levchenko, A.: Photogalvanic effect in Weyl semimetals. *Physical Review B* **96**, 075123 (2017). doi:[10.1103/PhysRevB.96.075123](https://doi.org/10.1103/PhysRevB.96.075123)
 161. Golub, L.E., Ivchenko, E.L., Spivak, B.Z.: Photocurrent in gyrotropic Weyl semimetals. *JETP Letters* **105**(12), 782–785 (2017). doi:[10.1134/S0021364017120062](https://doi.org/10.1134/S0021364017120062)
 162. Boyd, R.W.: *Nonlinear Optics*, 4th edn. Academic Press, San Diego (2020). doi:[10.1016/C2015-0-05510-1](https://doi.org/10.1016/C2015-0-05510-1)
 163. Sturman, B.I., Fridkin, V.M.: *The Photovoltaic and Photorefractive Effects in Noncentrosymmetric Materials*. Gordon and Breach Science Publishers, Philadelphia (1992)
 164. Sipe, J.E., Shkrebtii, A.I.: Second-order optical response in semiconductors. *Physical Review B* **61**(8), 5337–5352 (2000). doi:[10.1103/PhysRevB.61.5337](https://doi.org/10.1103/PhysRevB.61.5337)
 165. Rostami, H., Polini, M.: Nonlinear anomalous photocurrents in Weyl semimetals. *Physical Review B* **97**, 195151 (2018). doi:[10.1103/PhysRevB.97.195151](https://doi.org/10.1103/PhysRevB.97.195151)
 166. Shockley, W., Queisser, H.J.: Detailed balance limit of efficiency of p-n junction solar cells. *Journal of Applied Physics* **32**, 510–519 (1961). doi:[10.1063/1.1736034](https://doi.org/10.1063/1.1736034)
 167. Spanier, J.E., Fridkin, V.M., Rappe, A.M., Akbashev, A.R., Polemi, A., Qi, Y., Gu, Z., Young, S.M., Hawley, C.J., Imbrenda, D., Xiao, G., Bennett-Jackson, A.L., Johnson, C.L.: Power conversion efficiency exceeding the Shockley–Queisser limit in a ferroelectric insulator. *Nature Photonics* **10**, 611–616 (2016). doi:[10.1038/nphoton.2016.143](https://doi.org/10.1038/nphoton.2016.143)
 168. Osterhoudt, G.B., Diebel, L.K., Gray, M.J., Yang, X., Stanco, J., Huang, X., Shen, B., Ni, N., Moll, P.J.W., Ran, Y., Burch, K.S.: Colossal mid-infrared bulk photovoltaic effect in a type-I Weyl semimetal. *Nature Materials* **18**, 471–475 (2019). doi:[10.1038/s41563-019-0297-4](https://doi.org/10.1038/s41563-019-0297-4)
 169. Zhang, L., Chen, Z., Zhang, K., Wang, L., Xu, H., Han, L., Guo, W., Yang, Y., Kuo, C.-N., Lue, C.S., Mondal, D., Fuji, J., Vobornik, I., Ghosh, B., Agarwal, A., Xing, H., Chen, X., Politano, A., Lu, W.: High-frequency rectifiers based on type-II Dirac fermions. *Nature Communications* **12**(1), 1584 (2021). doi:[10.1038/s41467-021-21906-w](https://doi.org/10.1038/s41467-021-21906-w)
 170. Wang, L., Han, L., Guo, W., Zhang, L., Yao, C., Chen, Z., Chen, Y., Guo, C., Zhang, K., Kuo, C.-N., Lue, C.S., Politano, A., Xing, H., Jiang, M., Yu, X., Chen, X., Lu, W.: Hybrid Dirac semimetal-based photodetector with efficient low-energy photon harvesting. *Light: Science & Applications* **11**(1), 53 (2022). doi:[10.1038/s41377-022-00741-8](https://doi.org/10.1038/s41377-022-00741-8)
 171. Weng, H.: Lighting up Weyl semimetals. *Nature Materials* **18**, 428–429 (2019). doi:[10.1038/s41563-019-0330-7](https://doi.org/10.1038/s41563-019-0330-7)
 172. Glass, A.M., von der Linde, D., Negran, T.J.: High-voltage bulk photovoltaic effect and the photorefractive process in LiNbO₃. *Applied Physics Letters* **25**, 233–235 (1974). doi:[10.1063/1.1655453](https://doi.org/10.1063/1.1655453)
 173. Nastos, F., Sipe, J.E.: Optical rectification and shift currents in GaAs and GaP response: Below and above the band gap. *Physical Review B* **74**, 035201 (2006). doi:[10.1103/PhysRevB.74.035201](https://doi.org/10.1103/PhysRevB.74.035201)
 174. Laman, N., Shkrebtii, A.I., Sipe, J.E., van Driel, H.M.: Quantum interference control of currents in CdSe with a single optical beam. *Applied Physics Letters* **75**, 2581–2583 (1999). doi:[10.1063/1.125084](https://doi.org/10.1063/1.125084)
 175. Zhang, Y., Ishizuka, H., van den Brink, J., Felser, C., Yan, B., Nagaosa, N.: Photogalvanic effect in Weyl semimetals from first principles. *Physical Review B* **97**, 241118 (2018). doi:[10.1103/PhysRevB.97.241118](https://doi.org/10.1103/PhysRevB.97.241118)
 176. Sun, K., Sun, S.-S., Wei, L.-L., Guo, C., Tian, H.-F., Chen, G.-F., Yang, H.-X., Li, J.-Q.: Circular photogalvanic effect in the Weyl semimetal TaAs. *Chinese Physics Letters* **34**, 117203 (2017). doi:[10.1088/0256-307X/34/11/117203](https://doi.org/10.1088/0256-307X/34/11/117203)
 177. Ji, Z., Liu, G., Addison, Z., Liu, W., Yu, P., Gao, H., Liu, Z., Rappe, A.M., Kane, C.L., Mele, E.J., Agarwal, R.: Spatially dispersive circular photogalvanic effect in a Weyl semimetal. *Nature Materials* **18**, 955–962

- (2019). doi:[10.1038/s41563-019-0421-5](https://doi.org/10.1038/s41563-019-0421-5)
178. Gabor, N.M., Song, J.C.W., Ma, Q., Nair, N.L., Taychatanapat, T., Watanabe, K., Taniguchi, T., Levitov, L.S., Jarillo-Herrero, P.: Hot carrier-assisted intrinsic photoresponse in graphene. *Science* **334**, 648–652 (2011). doi:[10.1126/science.1211384](https://doi.org/10.1126/science.1211384)
 179. McIver, J.W., Hsieh, D., Steinberg, H., Jarillo-Herrero, P., Gedik, N.: Control over topological insulator photocurrents with light polarization. *Nature Nanotechnology* **7**, 96–100 (2012). doi:[10.1038/nnano.2011.214](https://doi.org/10.1038/nnano.2011.214)
 180. Yuan, H., Wang, X., Lian, B., Zhang, H., Fang, X., Shen, B., Xu, G., Xu, Y., Zhang, S.-C., Hwang, H.-Y., Cui, Y.: Generation and electric control of spin-valley-coupled circular photogalvanic current in WSe₂. *Nature Nanotechnology* **9**, 851–857 (2014). doi:[10.1038/nnano.2014.183](https://doi.org/10.1038/nnano.2014.183)
 181. Tan, L.-Z., Zheng, F., Young, S.M., Wang, F., Liu, S., Rappe, A.M.: Shift current bulk photovoltaic effect in polar materials—hybrid and oxide perovskites and beyond. *npj Computational Materials* **2**, 1–12 (2016). doi:[10.1038/npjcompumats.2016.26](https://doi.org/10.1038/npjcompumats.2016.26)
 182. Ibañez-Azpiroz, J., Tsirkin, S.S., Souza, I.: Ab initio calculation of the shift photocurrent by Wannier interpolation. *Physical Review B* **97**, 245143 (2018). doi:[10.1103/PhysRevB.97.245143](https://doi.org/10.1103/PhysRevB.97.245143)
 183. Lihm, J.-M.: Comment on “Ab initio calculation of the shift photocurrent by Wannier interpolation”. *Physical Review B* **103**, 247101 (2021). doi:[10.1103/PhysRevB.103.247101](https://doi.org/10.1103/PhysRevB.103.247101). [2105.14302](https://doi.org/10.1103/PhysRevB.103.247101)
 184. Côté, D., Laman, N., van Driel, H.M.: Rectification and shift currents in GaAs. *Applied Physics Letters* **80**, 905–907 (2002). doi:[10.1063/1.1436530](https://doi.org/10.1063/1.1436530)
 185. Ma, J., Gu, Q., Liu, Y., Lai, J., Yu, P., Zhuo, X., Liu, Z., Chen, J.-H., Feng, J., Sun, D.: Nonlinear photoresponse of type-II Weyl semimetals. *Nature Materials* **18**, 476–481 (2019). doi:[10.1038/s41563-019-0296-5](https://doi.org/10.1038/s41563-019-0296-5)
 186. Karplus, R., Luttinger, J.M.: Hall Effect in Ferromagnetics. *Physical Review* **95**, 1154–1160 (1954). doi:[10.1103/PhysRev.95.1154](https://doi.org/10.1103/PhysRev.95.1154)
 187. Sundaram, G., Niu, Q.: Wave-packet dynamics in slowly perturbed crystals: Gradient corrections and Berry-phase effects. *Physical Review B* **59**, 14915–14925 (1999). doi:[10.1103/PhysRevB.59.14915](https://doi.org/10.1103/PhysRevB.59.14915)
 188. Zhang, Y., Sun, Y., Yan, B.: Berry curvature dipole in Weyl semimetal materials: An ab initio study. *Physical Review B* **97**, 041101 (2018). doi:[10.1103/PhysRevB.97.041101](https://doi.org/10.1103/PhysRevB.97.041101)
 189. Gao, Y., Zhang, F., Zhang, W.: Second-order nonlinear Hall effect in Weyl semimetals. *Physical Review B* **102**(24), 245116 (2020). doi:[10.1103/PhysRevB.102.245116](https://doi.org/10.1103/PhysRevB.102.245116)
 190. Chang, G., Yin, J.-X., Neupert, T., Sanchez, D.S., Belopolski, I., Zhang, S.S., Cochran, T.A., Chéng, Z., Hsu, M.-C., Huang, S.-M., Lian, B., Xu, S.-Y., Lin, H., Hasan, M.Z.: Unconventional photocurrents from surface Fermi arcs in topological chiral semimetals. *Physical Review Letters* **124**(16), 166404 (2020). doi:[10.1103/PhysRevLett.124.166404](https://doi.org/10.1103/PhysRevLett.124.166404)
 191. Steiner, J.F., Andreev, A.V., Breitkreiz, M.: Surface photogalvanic effect in Weyl semimetals. *Physical Review Research* **4**(2), 023021 (2022). doi:[10.1103/PhysRevResearch.4.023021](https://doi.org/10.1103/PhysRevResearch.4.023021)
 192. Liang, L., Sukhachov, P.O., Balatsky, A.V.: Axial magnetoelectric effect in Dirac semimetals. *Physical Review Letters* **126**, 247202 (2021). doi:[10.1103/PhysRevLett.126.247202](https://doi.org/10.1103/PhysRevLett.126.247202)
 193. Lv, Y.-Y., Xu, J., Han, S., Zhang, C., Han, Y., Zhou, J., Yao, S.-H., Liu, X.-P., Lu, M.-H., Weng, H., Xie, Z., Chen, Y.B., Hu, J., Chen, Y.-F., Zhu, S.: High-harmonic generation in Weyl semimetal β -WP₂ crystals. *Nature Communications* **12**(1), 6437 (2021). doi:[10.1038/s41467-021-26766-y](https://doi.org/10.1038/s41467-021-26766-y)
 194. Allen, L., Beijersbergen, M.W., Spreeuw, R.J.C., Woerdman, J.P.: Orbital angular momentum of light and the transformation of Laguerre-Gaussian laser modes. *Physical Review A* **45**(11), 8185–8189 (1992). doi:[10.1103/PhysRevA.45.8185](https://doi.org/10.1103/PhysRevA.45.8185)
 195. Quinteiro, G.F., Tamborenea, P.I.: Theory of the optical absorption of light carrying orbital angular momentum by semiconductors. *EPL (Europhysics Letters)* **85**, 47001 (2009). doi:[10.1209/0295-5075/85/47001](https://doi.org/10.1209/0295-5075/85/47001)
 196. Lebedew, P.: Untersuchungen über die Druckkräfte des Lichtes. *Annalen der Physik* **311**, 433–458 (1901). doi:[10.1002/andp.19013111102](https://doi.org/10.1002/andp.19013111102)
 197. Patankar, S., Wu, L., Lu, B., Rai, M., Tran, J.D., Morimoto, T., Parker, D.E., Grushin, A.G., Nair, N.L., Analytis, J.G., Moore, J.E., Orenstein, J., Torchinsky, D.H.: Resonance-enhanced optical nonlinearity in the Weyl semimetal TaAs. *Physical Review B* **98**(16), 165113 (2018). doi:[10.1103/PhysRevB.98.165113](https://doi.org/10.1103/PhysRevB.98.165113)
 198. Gao, Y., Kaushik, S., Philip, E.J., Li, Z., Qin, Y., Liu, Y.P., Zhang, W.L., Su, Y.L., Chen, X., Weng, H.,

- Kharzeev, D.E., Liu, M.K., Qi, J.: Chiral terahertz wave emission from the Weyl semimetal TaAs. *Nature Communications* **11**, 720 (2020). doi:[10.1038/s41467-020-14463-1](https://doi.org/10.1038/s41467-020-14463-1)
199. van der Ziel, J.P., Pershan, P.S., Malmstrom, L.D.: Optically-induced magnetization resulting from the inverse Faraday effect. *Physical Review Letters* **15**(5), 190–193 (1965). doi:[10.1103/PhysRevLett.15.190](https://doi.org/10.1103/PhysRevLett.15.190)
200. Hertel, R.: Theory of the inverse Faraday effect in metals. *Journal of Magnetism and Magnetic Materials* **303**(1), 1–4 (2006). doi:[10.1016/j.jmmm.2005.10.225](https://doi.org/10.1016/j.jmmm.2005.10.225)
201. Pershan, P.S.: Nonlinear optical properties of solids: Energy considerations. *Physical Review* **130**(3), 919–929 (1963). doi:[10.1103/PhysRev.130.919](https://doi.org/10.1103/PhysRev.130.919)
202. Kimel, A.V., Kirilyuk, A., Usachev, P.A., Pisarev, R.V., Balbashov, A.M., Rasing, T.: Ultrafast non-thermal control of magnetization by instantaneous photomagnetic pulses. *Nature* **435**(7042), 655–657 (2005). doi:[10.1038/nature03564](https://doi.org/10.1038/nature03564)
203. Kimel, A.V., Kirilyuk, A., Rasing, T.: Femtosecond opto-magnetism: Ultrafast laser manipulation of magnetic materials. *Laser & Photonics Reviews* **1**(3), 275–287 (2007). doi:[10.1002/lpor.200710022](https://doi.org/10.1002/lpor.200710022)
204. Zyuzin, A.A., Silaev, M., Zyuzin, V.A.: Nonlinear chiral transport in Dirac semimetals. *Physical Review B* **98**, 205149 (2018). doi:[10.1103/PhysRevB.98.205149](https://doi.org/10.1103/PhysRevB.98.205149)
205. Kawaguchi, M., Hirose, H., Chi, Z., Lau, Y.-C., Freimuth, F., Hayashi, M.: Giant Inverse Faraday Effect in Dirac Semimetals. *arXiv* (2020). [2009.01388](https://arxiv.org/abs/2009.01388)
206. Tokman, I.D., Chen, Q., Shereshevsky, I.A., Pozdnyakova, V.I., Oladyskin, I., Tokman, M., Belyanin, A.: Inverse Faraday effect in graphene and Weyl semimetals. *Physical Review B* **101**, 174429 (2020). doi:[10.1103/PhysRevB.101.174429](https://doi.org/10.1103/PhysRevB.101.174429)
207. Gao, Y., Wang, C., Xiao, D.: Topological inverse Faraday effect in Weyl semimetals. *arXiv* (2020). [2009.13392](https://arxiv.org/abs/2009.13392)
208. Cao, J., Zeng, C., Li, X.-P., Wang, M., Yang, S.A., Yu, Z.-M., Yao, Y.: Low-Frequency Divergence of Circular Photomagnetic Effect in Topological Semimetals. *arXiv* (2022). [2201.06243](https://arxiv.org/abs/2201.06243)
209. Ghimire, S., DiChiara, A.D., Sistrunk, E., Agostini, P., DiMauro, L.F., Reis, D.A.: Observation of high-order harmonic generation in a bulk crystal. *Nature Physics* **7**, 138–141 (2011). doi:[10.1038/nphys1847](https://doi.org/10.1038/nphys1847)
210. Liu, H., Li, Y., You, Y.S., Ghimire, S., Heinz, T.F., Reis, D.A.: High-harmonic generation from an atomically thin semiconductor. *Nature Physics* **13**, 262–265 (2017). doi:[10.1038/nphys3946](https://doi.org/10.1038/nphys3946)
211. Liu, H., Guo, C., Vampa, G., Zhang, J.L., Sarmiento, T., Xiao, M., Bucksbaum, P.H., Vučković, J., Fan, S., Reis, D.A.: Enhanced high-harmonic generation from an all-dielectric metasurface. *Nature Physics* **14**, 1006–1010 (2018). doi:[10.1038/s41567-018-0233-6](https://doi.org/10.1038/s41567-018-0233-6)
212. Goulielmakis, E., Brabec, T.: High harmonic generation in condensed matter. *Nature Photonics* **16**, 411–421 (2022). doi:[10.1038/s41566-022-00988-y](https://doi.org/10.1038/s41566-022-00988-y)
213. Bai, Y., Fei, F., Wang, S., Li, N., Li, X., Song, F., Li, R., Xu, Z., Liu, P.: High-harmonic generation from topological surface states. *Nature Physics* **17**, 311–315 (2021). doi:[10.1038/s41567-020-01052-8](https://doi.org/10.1038/s41567-020-01052-8)
214. Heide, C., Kobayashi, Y., Baykusheva, D.R., Jain, D., Sobota, J.A., Hashimoto, M., Kirchmann, P.S., Oh, S., Heinz, T.F., Reis, D.A., Ghimire, S.: Probing topological phase transitions using high-harmonic generation. *Nature Photonics*, 1–5 (2022). doi:[10.1038/s41566-022-01050-7](https://doi.org/10.1038/s41566-022-01050-7)
215. Luu, T.T., Wörner, H.J.: Measurement of the Berry curvature of solids using high-harmonic spectroscopy. *Nature Communications* **9**, 916 (2018). doi:[10.1038/s41467-018-03397-4](https://doi.org/10.1038/s41467-018-03397-4)
216. Zhong, S., Moore, J.E., Souza, I.: Gyrotropic magnetic effect and the magnetic moment on the Fermi surface. *Physical Review Letters* **116**(7), 077201 (2016). doi:[10.1103/PhysRevLett.116.077201](https://doi.org/10.1103/PhysRevLett.116.077201)
217. Chan, C.-K., Lee, P.A., Burch, K.S., Han, J.H., Ran, Y.: When chiral photons meet chiral fermions: Photoinduced anomalous Hall effects in Weyl semimetals. *Physical Review Letters* **116**(2), 026805 (2016). doi:[10.1103/PhysRevLett.116.026805](https://doi.org/10.1103/PhysRevLett.116.026805)
218. Nathan, F., Martin, I., Refael, G.: Topological Frequency Conversion in Weyl Semimetals. *arXiv* (2022). [2201.07804](https://arxiv.org/abs/2201.07804)
219. Ishizuka, H., Hayata, T., Ueda, M., Nagaosa, N.: Emergent electromagnetic induction and adiabatic charge pumping in noncentrosymmetric Weyl semimetals. *Physical Review Letters* **117**(21), 216601 (2016). doi:[10.1103/PhysRevLett.117.216601](https://doi.org/10.1103/PhysRevLett.117.216601)
220. Ishizuka, H., Hayata, T., Ueda, M., Nagaosa, N.: Momentum-space electromagnetic induction in Weyl semimetals. *Physical Review B* **95**(24), 245211 (2017). doi:[10.1103/PhysRevB.95.245211](https://doi.org/10.1103/PhysRevB.95.245211)

221. Halterman, K., Alidoust, M., Zyuzin, A.: Epsilon-near-zero response and tunable perfect absorption in Weyl semimetals. *Physical Review B* **98**(8), 085109 (2018). doi:[10.1103/PhysRevB.98.085109](https://doi.org/10.1103/PhysRevB.98.085109)
222. Zhao, C., Zhao, C., Hu, G., Chen, Y., Zhang, Q., Zhang, Y., Zhang, Y., Qiu, C.-W., Qiu, C.-W.: Unidirectional bound states in the continuum in Weyl semimetal nanostructures. *Photonics Research* **10**(8), 1828–1838 (2022). doi:[10.1364/PRJ.459383](https://doi.org/10.1364/PRJ.459383)
223. Liu, M.Q., Zhao, C.Y., Bao, H.: Transverse Kerker scattering governed by two nondegenerate electric dipoles and its application in arbitrary beam steering. *Journal of Quantitative Spectroscopy and Radiative Transfer* **262**, 107514 (2021). doi:[10.1016/j.jqsrt.2021.107514](https://doi.org/10.1016/j.jqsrt.2021.107514)
224. Oktay, G., Sarisaman, M., Tas, M.: Lasing with topological Weyl semimetal. *Scientific Reports* **10**, 3127 (2020). doi:[10.1038/s41598-020-59423-3](https://doi.org/10.1038/s41598-020-59423-3)
225. Chen, G.: *Nanoscale Energy Transport and Conversion: A Parallel Treatment of Electrons, Molecules, Phonons, and Photons*. Oxford University Press, Oxford (2005)
226. Zhang, Z.M.: *Nano/Microscale Heat Transfer*. McGraw-Hill, New York (2007)
227. Bergman, T.L., Bergman, T.L., Incropera, F.P., Dewitt, D.P., Lavine, A.S.: *Fundamentals of Heat and Mass Transfer*. John Wiley & Sons, Hoboken (2011)
228. Modest, M.F., Mazumder, S.: *Radiative Heat Transfer*. Academic Press, London (2021)
229. Howell, J.R., Mengüç, M.P., Daun, K., Siegel, R.: *Thermal Radiation Heat Transfer*. CRC press, London (2020)
230. Snyder, W.C., Wan, Z., Li, X.: Thermodynamic constraints on reflectance reciprocity and Kirchhoff's law. *Applied Optics* **37**, 3464–3470 (1998). doi:[10.1364/AO.37.003464](https://doi.org/10.1364/AO.37.003464)
231. Zhao, B., Shi, Y., Wang, J., Zhao, Z., Zhao, N., Fan, S.: Near-complete violation of Kirchhoff's law of thermal radiation with a 0.3 T magnetic field. *Optics Letters* **44**, 4203–4206 (2019). doi:[10.1364/OL.44.004203](https://doi.org/10.1364/OL.44.004203)
232. Onsager, L.: Reciprocal relations in irreversible processes. I. *Physical Review* **37**(4), 405–426 (1931). doi:[10.1103/PhysRev.37.405](https://doi.org/10.1103/PhysRev.37.405)
233. Onsager, L.: Reciprocal relations in irreversible processes. II. *Physical Review* **38**(12), 2265–2279 (1931). doi:[10.1103/PhysRev.38.2265](https://doi.org/10.1103/PhysRev.38.2265)
234. Madelung, O.: *Semiconductors: Data Handbook*. Springer, Berlin (2004)
235. Tanner, D.B.: *Optical Effects in Solids*. Cambridge University Press, Cambridge (2019)
236. Zhu, L., Fan, S.: Near-complete violation of detailed balance in thermal radiation. *Physical Review B* **90**, 220301 (2014). doi:[10.1103/PhysRevB.90.220301](https://doi.org/10.1103/PhysRevB.90.220301)
237. Coey, J.M.D.: *Magnetism and Magnetic Materials*. Cambridge University Press, Cambridge (2010)
238. Feng, W., Fu, X., Wan, C., Yuan, Z., Han, X., Quang, N.V., Cho, S.: Spin gapless semiconductor like Ti_2MnAl film as a new candidate for spintronics application. *physica status solidi (RRL) – Rapid Research Letters* **9**, 641–645 (2015). doi:[10.1002/pssr.201510340](https://doi.org/10.1002/pssr.201510340)
239. Shi, W., Muechler, L., Manna, K., Zhang, Y., Koepnik, K., Car, R., van den Brink, J., Felser, C., Sun, Y.: Prediction of a magnetic Weyl semimetal without spin-orbit coupling and strong anomalous Hall effect in the Heusler compensated ferrimagnet Ti_2MnAl . *Physical Review B* **97**, 060406 (2018). doi:[10.1103/PhysRevB.97.060406](https://doi.org/10.1103/PhysRevB.97.060406)
240. Wu, J., Wang, Z., Zhai, H., Shi, Z., Wu, X., Wu, X., Wu, F., Wu, F.: Near-complete violation of Kirchhoff's law of thermal radiation in ultrathin magnetic Weyl semimetal films. *Optical Materials Express* **11**, 4058–4066 (2021). doi:[10.1364/OME.444308](https://doi.org/10.1364/OME.444308)
241. Wu, X., Yu, H., Wu, F., Wu, B.: Enhanced nonreciprocal radiation in Weyl semimetals by attenuated total reflection. *AIP Advances* **11**, 075106 (2021). doi:[10.1063/5.0055418](https://doi.org/10.1063/5.0055418)
242. Wu, J., Wu, B., Wang, Z., Wu, X.: Strong nonreciprocal thermal radiation in Weyl semimetal-dielectric multilayer structure. *International Journal of Thermal Sciences* **181**, 107788 (2022). doi:[10.1016/j.ijthermalsci.2022.107788](https://doi.org/10.1016/j.ijthermalsci.2022.107788)
243. Zhao, B., Wang, J., Zhao, Z., Guo, C., Yu, Z., Fan, S.: Nonreciprocal thermal emitters using metasurfaces with multiple diffraction channels. *Physical Review Applied* **16**, 064001 (2021). doi:[10.1103/PhysRevApplied.16.064001](https://doi.org/10.1103/PhysRevApplied.16.064001)
244. Maghrebi, M.F., Gorshkov, A.V., Sau, J.D.: Fluctuation-induced torque on a topological insulator out of thermal equilibrium. *Physical Review Letters* **123**, 055901 (2019). doi:[10.1103/PhysRevLett.123.055901](https://doi.org/10.1103/PhysRevLett.123.055901)

245. Khan, E., Narimanov, E.E.: Spinning radiation from a topological insulator. *Physical Review B* **100**, 081408 (2019). doi:[10.1103/PhysRevB.100.081408](https://doi.org/10.1103/PhysRevB.100.081408)
246. Wang, Y., Khandekar, C., Gao, X., Li, T., Jiao, D., Jacob, Z.: Broadband circularly polarized thermal radiation from magnetic Weyl semimetals. *Opt. Mater. Express* **11**(11), 3880–3895 (2021). doi:[10.1364/OME.437838](https://doi.org/10.1364/OME.437838)
247. Khandekar, C., Khosravi, F., Li, Z., Jacob, Z.: New spin-resolved thermal radiation laws for nonreciprocal bianisotropic media. *New Journal of Physics* **22**(12), 123005 (2020). doi:[10.1088/1367-2630/abc988](https://doi.org/10.1088/1367-2630/abc988)
248. Ott, A., Ben-Abdallah, P., Biehs, S.-A.: Circular heat and momentum flux radiated by magneto-optical nanoparticles. *Physical Review B* **97**, 205414 (2018). doi:[10.1103/PhysRevB.97.205414](https://doi.org/10.1103/PhysRevB.97.205414)
249. Guo, Y., Fan, S.: Single gyrotropic particle as a heat engine. *ACS Photonics* **8**, 1623–1629 (2021). doi:[10.1021/acsp Photonics.0c01920](https://doi.org/10.1021/acsp Photonics.0c01920)
250. Zhu, L., Fan, S.: Persistent directional current at equilibrium in nonreciprocal many-body near field electromagnetic heat transfer. *Physical Review Letters* **117**, 134303 (2016). doi:[10.1103/PhysRevLett.117.134303](https://doi.org/10.1103/PhysRevLett.117.134303)
251. Ott, A., Biehs, S.-A., Ben-Abdallah, P.: Anomalous photon thermal Hall effect. *Physical Review B* **101**, 241411 (2020). doi:[10.1103/PhysRevB.101.241411](https://doi.org/10.1103/PhysRevB.101.241411)
252. Guo, C., Zhao, B., Huang, D., Fan, S.: Radiative thermal router based on tunable magnetic Weyl semimetals. *ACS Photonics* **7**(11), 3257–3263 (2020). doi:[10.1021/acsp Photonics.0c01376](https://doi.org/10.1021/acsp Photonics.0c01376)
253. Fan, S.: Thermal photonics and energy applications. *Joule* **1**, 264–273 (2017). doi:[10.1016/j.joule.2017.07.012](https://doi.org/10.1016/j.joule.2017.07.012)
254. Silveirinha, M.G.: Topological angular momentum and radiative heat transport in closed orbits. *Physical Review B* **95**, 115103 (2017). doi:[10.1103/PhysRevB.95.115103](https://doi.org/10.1103/PhysRevB.95.115103)
255. Khandekar, C., Jacob, Z.: Thermal spin photonics in the near-field of nonreciprocal media. *New Journal of Physics* **21**(10), 103030 (2019). doi:[10.1088/1367-2630/ab494d](https://doi.org/10.1088/1367-2630/ab494d)
256. Guo, C., Guo, Y., Fan, S.: Relation between photon thermal Hall effect and persistent heat current in nonreciprocal radiative heat transfer. *Physical Review B* **100**, 205416 (2019). doi:[10.1103/PhysRevB.100.205416](https://doi.org/10.1103/PhysRevB.100.205416)
257. Guo, C., Fan, S.: Theoretical constraints on reciprocal and non-reciprocal many-body radiative heat transfer. *Physical Review B* **102**, 085401 (2020). doi:[10.1103/PhysRevB.102.085401](https://doi.org/10.1103/PhysRevB.102.085401)
258. Ben-Abdallah, P.: Photon thermal Hall effect. *Physical Review Letters* **116**, 084301 (2016). doi:[10.1103/PhysRevLett.116.084301](https://doi.org/10.1103/PhysRevLett.116.084301)
259. Otey, C.R., Lau, W.T., Fan, S.: Thermal rectification through vacuum. *Physical Review Letters* **104**, 154301 (2010). doi:[10.1103/PhysRevLett.104.154301](https://doi.org/10.1103/PhysRevLett.104.154301)
260. Ott, A., Messina, R., Ben-Abdallah, P., Biehs, S.-A.: Radiative thermal diode driven by nonreciprocal surface waves. *Applied Physics Letters* **114**(16), 163105 (2019). doi:[10.1063/1.5093626](https://doi.org/10.1063/1.5093626)
261. Wang, K., Gao, L.: High-Efficient Photonic Thermal Rectification with Magnetocontrollability. *ES Energy & Environment* **7**, 12–16 (2020). doi:[10.30919/eseec350](https://doi.org/10.30919/eseec350)
262. Ott, A., Biehs, S.-A.: Thermal rectification and spin-spin coupling of nonreciprocal localized and surface modes. *Physical Review B* **101**, 155428 (2020). doi:[10.1103/PhysRevB.101.155428](https://doi.org/10.1103/PhysRevB.101.155428)
263. Tang, G., Chen, J., Zhang, L.: Twist-induced control of near-field heat radiation between magnetic Weyl semimetals. *ACS Photonics* **8**(2), 443–448 (2021). doi:[10.1021/acsp Photonics.0c01945](https://doi.org/10.1021/acsp Photonics.0c01945)
264. Xu, G., Sun, J., Mao, H.: Near-field radiative thermal modulation between Weyl semimetal slabs. *Journal of Quantitative Spectroscopy and Radiative Transfer* **253**, 107173 (2020). doi:[10.1016/j.jqsrt.2020.107173](https://doi.org/10.1016/j.jqsrt.2020.107173)
265. Abraham Ekeroth, R.M., Ben-Abdallah, P., Cuevas, J.C., García-Martín, A.: Anisotropic thermal magnetoresistance for an active control of radiative heat transfer. *ACS Photonics* **5**(3), 705–710 (2018). doi:[10.1021/acsp Photonics.7b01223](https://doi.org/10.1021/acsp Photonics.7b01223)
266. Zhu, L., Guo, Y., Fan, S.: Theory of many-body radiative heat transfer without the constraint of reciprocity. *Physical Review B* **97**, 094302 (2018). doi:[10.1103/PhysRevB.97.094302](https://doi.org/10.1103/PhysRevB.97.094302)
267. Fan, L., Guo, Y., Papadakis, G.T., Zhao, B., Zhao, Z., Buddhiraju, S., Orenstein, M., Fan, S.: Nonreciprocal radiative heat transfer between two planar bodies. *Physical Review B* **101**, 085407 (2020). doi:[10.1103/PhysRevB.101.085407](https://doi.org/10.1103/PhysRevB.101.085407)
268. Tsurimaki, Y., Qian, X., Pajovic, S., Boriskina, S., Chen, G.: Casimir Force among Spheres Made of Weyl Semimetals Breaking Lorentz Reciprocity. *arXiv* (2021). [2109.03809](https://arxiv.org/abs/2109.03809)

269. Wilson, J.H., Allocca, A.A., Galitski, V.: Repulsive Casimir force between Weyl semimetals. *Physical Review B* **91**, 235115 (2015). doi:[10.1103/PhysRevB.91.235115](https://doi.org/10.1103/PhysRevB.91.235115)
270. Farias, M.B., Zyuzin, A.A., Schmidt, T.L.: Casimir force between Weyl semimetals in a chiral medium. *Physical Review B* **101**, 235446 (2020). doi:[10.1103/PhysRevB.101.235446](https://doi.org/10.1103/PhysRevB.101.235446)
271. Chen, L., Chang, K.: Chiral-anomaly-driven Casimir-Lifshitz torque between Weyl semimetals. *Physical Review Letters* **125**, 047402 (2020). doi:[10.1103/PhysRevLett.125.047402](https://doi.org/10.1103/PhysRevLett.125.047402)
272. Rodriguez-Lopez, P., Popescu, A., Fialkovsky, I., Khusnutdinov, N., Woods, L.M.: Signatures of complex optical response in Casimir interactions of type I and II Weyl semimetals. *Communications Materials* **1**, 1–9 (2020). doi:[10.1038/s43246-020-0015-4](https://doi.org/10.1038/s43246-020-0015-4)
273. Boyer, T.H.: Van der Waals forces and zero-point energy for dielectric and permeable materials. *Physical Review A* **9**, 2078–2084 (1974). doi:[10.1103/PhysRevA.9.2078](https://doi.org/10.1103/PhysRevA.9.2078)
274. Tse, W.-K., MacDonald, A.H.: Quantized Casimir force. *Physical Review Letters* **109**, 236806 (2012). doi:[10.1103/PhysRevLett.109.236806](https://doi.org/10.1103/PhysRevLett.109.236806)
275. Grushin, A.G., Cortijo, A.: Tunable Casimir repulsion with three-dimensional topological insulators. *Physical Review Letters* **106**, 020403 (2011). doi:[10.1103/PhysRevLett.106.020403](https://doi.org/10.1103/PhysRevLett.106.020403)
276. Gelbwaser-Klimovsky, D., Graham, N., Kardar, M., Krüger, M.: Near field propulsion forces from nonreciprocal media. *Physical Review Letters* **126**, 170401 (2021). doi:[10.1103/PhysRevLett.126.170401](https://doi.org/10.1103/PhysRevLett.126.170401)